Convergent margin Ni-Cu-PGE-Cr ore systems: U-Pb petrochronology and environments of Cu-PGE versus Cr-PGE mineralization in Alaskan-type intrusions

Graham T. Nixon[1*], James S. Scoates[2], Dejan Milidragovic[1], James Nott[2], Nichole Moerhuis[2], Thomas J. Ver Hoeve[2], Matthew J. Manor[2†], and Ingrid M. Kjarsgaard[3]

[1]British Columbia Geological Survey, Ministry of Energy, Mines and Petroleum Resources, PO Box 9333 Stn Prov Govt, Victoria, British Columbia V8W 9N3

[2]Pacific Centre for Isotopic and Geochemical Research (PCIGR), Department of Earth, Ocean and Atmospheric Sciences, 2020-2207 Main Mall, University of British Columbia, Vancouver, British Columbia V6T 1Z4

[3]Consulting Mineralogist, 15 Scotia Place, Ottawa, Ontario K1S 0W2

†Present address: Department of Earth Sciences, 9 Arctic Avenue, Memorial University of Newfoundland, St. John's, Newfoundland A1B 3X5

*Corresponding author's e-mail:graham.nixon@gov.bc.ca

ABSTRACT

Magmatic Ni-Cu-PGE deposits hosted by ultramafic-mafic intrusions in convergent margin or supra-subduction/post-subduction tectonic settings are becoming an increasingly important global resource. In the northern Cordillera, this class of intrusions is restricted to the accreted arc terranes of the continental margin of North America where the Alaskan-type subclass is particularly prevalent. This report describes recent research on the Tulameen and Polaris Alaskan-type intrusions in British Columbia that contain orthomagmatic Ni-Cu-PGE mineralization. Preliminary U-Pb geochronological results and trace element analyses of zircon from the Tulameen intrusion are interpreted using an integrated petrochronological approach to distinguish crystallization from post-crystallization events and to constrain the duration of magmatism.

Magmatic Cu-PGE mineralization (predominantly chalcopyrite-bornite) in the Tulameen intrusion is hosted by hornblende-magnetite-bearing ultramafic rocks near its periphery. Preliminary results suggest that emplacement and crystallization of the Tulameen intrusion occurred ca. 204–205 Ma (latest Triassic), coincident with a 6 million year period centred on 205 Ma that produced the most important porphyry Cu-Au deposits in British Columbia. The Cu-PGE mineralization constitutes a unique deposit type for Alaskan-type intrusions and has some attributes in common with stratiform or 'reef-style' mineralization in tholeiitic layered intrusions.

Magmatic Ni-Cu-PGE sulphides (mainly pyrrhotite, chalcopyrite, minor pentlandite) in the Early Jurassic (ca. 186 Ma) Polaris intrusion are hosted by the more evolved ultramafic and mafic rocks. Remobilized ultramafic cumulates form a distinctive component of both intrusions: plastically deformed and dismembered olivine-chromite cumulates are widely distributed in dunite, and what are interpreted as synmagmatic avalanche deposits are well exposed at Tulameen. The remobilization of pre-existing cumulate sequences is rationalized in terms of an open-system magma recharge model that accounts for some of the key textural features exhibited by ultramafic rocks in Alaskan-type intrusions.

INTRODUCTION

The most important Ni-Cu-platinum group element (PGE) resources on Earth are hosted by ultramafic-mafic intrusions and volcanic rocks in various rift-related tectonic settings (e.g. Naldrett, 2004). In the past, magmatic Ni-Cu-PGE sulphide deposits at convergent margins have been regarded as unfavourable environments for nickel exploration due to a perceived lack of economically exploitable deposits. However, over the last 15 years or so, discoveries of significant Ni-sulphide deposits in convergent margin or supra-subduction/post-subduction settings have established this class of intrusions as an increasingly important economic resource. For example, production at the Carboniferous Aguablanca deposit in the Variscan orogenic belt in Spain, Europe's only orthomagmatic nickel mine, began in 2004 with a resource of 15.7 million metric tonnes (Mt) at 0.66 wt% Ni, 0.46 wt% Cu, and 0.47 g/t PGE (Piña, 2019); the Silurian-Devonian Xiarihamu deposit in the Central Asian Orogenic Belt (Eastern Kunlun arc terrane), the second largest Ni-sulphide deposit in China, constitutes a resource of 157 Mt at an average grade of 0.65 wt% Ni, 0.14 wt% Cu, and 0.013 wt% Co (Li et al., 2015; Song et al., 2016).

Nixon, G.T., Scoates, J.S., Milidragovic, D., Nott, J., Moerhuis, N., Ver Hoeve, T.J., Manor, M.J., and Kjarsgaard, I.M., 2020. Convergent margin Ni-Cu-PGE-Cr ore systems: U-Pb petrochronology and environments of Cu-PGE versus Cr-PGE mineralization in Alaskan-type intrusions; *in* Targeted Geoscience Initiative 5: Advances in the understanding of Canadian Ni-Cu-PGE and Cr ore systems – Examples from the Midcontinent Rift, the Circum-Superior Belt, the Archean Superior Province, and Cordilleran Alaskan-type intrusions, (ed.) W. Bleeker and M.G. Houlé; Geological Survey of Canada, Open File 8722, p. 197–218. https://doi.org/10.4095/326897

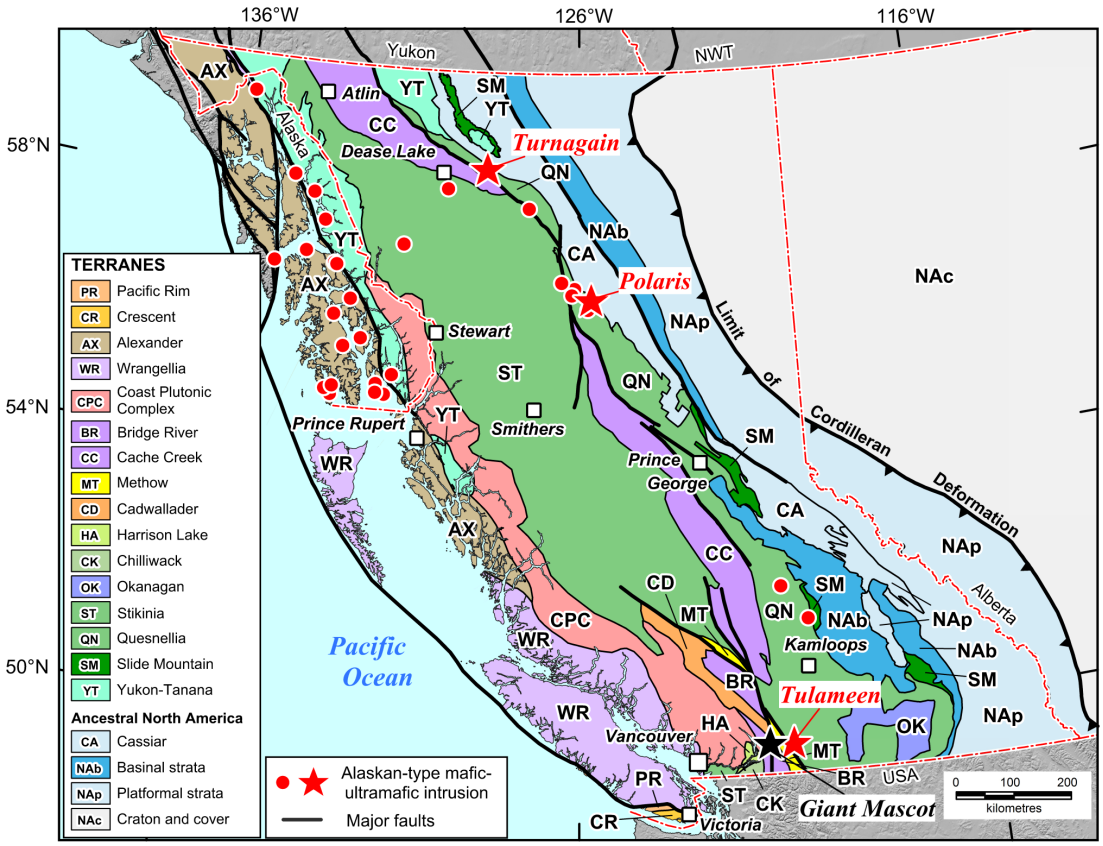

Figure 1. Terrane map of British Columbia and southeastern Alaska (*after* Colpron and Nelson, 2011) showing the distribution of Alaskan-type intrusions (*after* Himmelberg and Loney, 1995; Nixon et al., 1997). Current research on the Tulameen and Polaris intrusions is documented in this report. The subjects of previous studies, the Turnagain Alaskan-type intrusion (Scheel, 2007; Jackson-Brown, 2017; Nixon et al., 2020) and Late Cretaceous Giant Mascot ultramafic-mafic intrusion and Ni-Cu-PGE deposit (black star; Manor et al., 2016, 2017) are shown for reference. The Giant Mascot intrusion contains abundant orthopyroxene and is not an Alaskan-type body according to the mineralogical classification used in this report (Irvine, 1974; Nixon et al., 2015).

An overview of the characteristics and global distribution of Neoarchean to Mesozoic ultramafic-mafic intrusions with Ni-Cu-PGE mineralization in convergent margin settings is given by Nixon et al. (2015), who recognized two principal mineralogical subtypes of convergent-margin intrusions: Alaskan-type intrusions, which characteristically lack orthopyroxene (Irvine, 1974); and intrusions that carry abundant cumulus and/or postcumulus orthopyroxene. Both subtypes may exhibit a zonal arrangement of lithologies extending from dunite in the core of the intrusive body through orthopyroxene-bearing (harzburgite/lherzolite) or orthopyroxene-free (wehrlite) peridotite to hornblende-bearing pyroxenite and hornblendite±gabbro at the margin. The type example of a zoned, orthopyroxene-rich ultramafic body in British Columbia that hosts Ni-sulphide mineralization is the Late Cretaceous (ca. 93 Ma) Giant Mascot intrusion (Fig. 1). The Giant Mascot Ni-Cu sulphide deposit, the province's only former nickel mine (1958–1974), produced 4.2 Mt of ore grading 0.77 wt% Ni and 0.34 wt% Cu (Pinsent, 2002) from a series of subvertical ore shoots interpreted as representing conduit-style mineralization (Manor et al., 2016, 2017).

Regardless of tectonic setting, magmatic Ni-Cu-PGE deposits may be divided into two major groups: deposits mined primarily for their Ni and Cu, which tend to be rich in sulphide (10–90 vol.%, comprising mainly pyrrhotite, pentlandite, chalcopyrite, and minor pyrite); and PGE-rich deposits that are typically poor in sulphides (<0.1–5 vol.%; e.g. Naldrett, 2004; Maier, 2005). Alaskan-type intrusive suites are commonly perceived to evolve in sulphide-deficient magmatic environments and are primarily known for their chromitite-PGE mineralization in the dunite core and derivative platinum placers, some of which have been exploited economically (e.g. Tulameen, Nixon et al., 1990; *see* also reviews by Johan, 2002 and Weiser, 2002). In British Columbia, Late Triassic to Early Jurassic Alaskan-type intrusions are well represented in the accreted arc terranes of Quesnellia and Stikinia (Nixon et al., 1997; Fig. 1).

Perhaps in recognition of the growing economic potential of ultramafic-mafic intrusions at convergent margins, Naldrett (2010) introduced a new class of Ni-Cu sulphide deposit (NC-7, Ural-Alaskan-type) in his petrotectonic classification scheme, and cited the Early

Jurassic Turnagain ultramafic-mafic intrusion in northern British Columbia as the type example (Fig. 1). The Turnagain intrusion contains a large-tonnage, low-grade Ni-sulphide resource of 1842 Mt at an average grade of 0.21 wt% Ni and 0.013 wt% Co, and ranks ninth in the world for contained Ni metal (Scheel, 2007; Mudd and Jowitt, 2014). The unusual, currently subeconomic endowment of Ni-sulphide mineralization at Turnagain has been related to contamination of primitive high-Mg magmas by carbonaceous and sulphide-bearing sedimentary wallrocks that are also implicated in the origin of Cu-PGE mineralization in a younger intrusive phase (Nixon, 1998; Scheel, 2007; Jackson-Brown, 2017). Crustal contamination has also played an important role in the genesis of the Ni-Cu ores hosted by orthopyroxene-rich cumulates in the Giant Mascot deposit (Manor et al., 2016).

One prime objective of our studies of ultramafic-mafic intrusions at convergent margins is to establish the nature and timing of Ni-Cu-PGE mineralization within the context of the temporal and magmatic evolution of the host intrusion. Recently completed U-Pb and $^{40}Ar/^{39}Ar$ geochronological studies of the Turnagain intrusion have provided the first published absolute calibration of the multistage assembly of a zoned Alaskan-type intrusion (Nixon et al., 2020). The Turnagain body is a composite intrusion comprising four compositionally, spatially, and temporally distinct intrusive phases that were emplaced over approximately 4 million years in the Early Jurassic (ca. 189–185 Ma), concomitant with the accretion of major arc terranes in the northern Cordillera (Nixon et al., 2020). The main Ni resource given above is hosted by early stage dunite-wehrlite-clinopyroxenite cumulates (Scheel, 2007), whereas Cu-PGE mineralization is restricted to the youngest clinopyroxenite-hornblendite-(wehrlite-leucodiorite) intrusive component of the complex (Jackson-Brown, 2017).

This report describes recent work on the Tulameen and Polaris Alaskan-type intrusions in British Columbia (Fig. 1). Herein, we (1) present preliminary high-precision U-Pb crystallization ages and trace element concentrations of zircon from the Tulameen intrusion and frame them in an integrated petrochronological context; (2) describe the textures and mineralogy of a zone of Cu-PGE mineralization hosted by evolved ultramafic rocks in the Tulameen intrusion, mineralization that has affinities with stratiform Cu-PGE horizons in layered intrusions; and (3) adopt a magma recharge model to rationalize the physical reworking of cumulate sequences in the core of the Tulameen and Polaris intrusions. The results have significant implications for Ni-Cu-PGE exploration in convergent margin settings, and specifically for Alaskan-type intrusive complexes.

TULAMEEN INTRUSION

The Late Triassic Tulameen ultramafic-mafic intrusion (60 km^2) in southern British Columbia (Fig. 1) is a classically zoned Alaskan-type intrusion with a dunite core passing outwards through olivine clinopyroxenite/clinopyroxenite to hornblende clinopyroxenite and hornblendite at the margin (Findlay, 1963, 1969; Fig. 2). Gabbroic rocks are widely distributed, though concentrated in the eastern, central, and south-central parts of the intrusion, and a voluminous dioritic phase occupies the southeastern margin (Fig. 2). The intrusion has a dyke- or sill-like form (18 km long x 6 km maximum width) that is broadly concordant with the regional structural grain. Bedding attitudes in metavolcanic and metasedimentary host rocks of the Upper Triassic Nicola Group strike north-northwesterly and dip moderately to steeply (40–70°) to the west (Nixon, 2018). Contacts with the Nicola Group are defined by ductile (mylonitic) and brittle fault zones (Nixon and Rublee, 1988; Rublee, 1989). Rafts of hornfelsed metasedimentary rocks correlated with the Nicola Group occur within the Tulameen intrusion and establish the intrusive nature of the complex. A post-Triassic upper greenschist to lower amphibolite facies metamorphism in the Nicola Group overprints the Tulameen intrusion. The age of the metamorphism is considered to be broadly synchronous with the intrusion of the Eagle granodiorite-tonalite pluton situated a kilometre to the west (Greig et al., 1992). The pluton has been dated by U-Pb (zircon) at ca. 148–157 Ma (Late Jurassic: Greig et al., 1992).

In the following sections, we (1) present new petrochronological results for the Tulameen intrusion and discuss their significance; (2) illustrate the textural features of remobilized chromitites in the dunite core and fragmental dunite-clinopyroxenite cumulates peripheral to the core that are interpreted as magmatic avalanche deposits; and (3) describe the nature of recently discovered Cu-PGE mineralization in the Tulameen intrusion, and compare this Alaskan-type mineral occurrence with a specific type of stratiform or 'reef-style' mineralization hosted by layered intrusions.

Petrochronology

A framework for the crystallization history of the Tulameen intrusion is being established and refined using a petrochronological approach by combining scanning electron microscope-cathodoluminescence (SEM-CL) imaging, laser ablation-inductively coupled plasma-mass spectrometry (LA-ICP-MS) trace element analysis, and chemical abrasion-isotope dilution-thermal ionization mass spectrometry (CA-ID-TIMS) of individual zircon crystals or fragments thereof. Petrochronology links the petrology and geochemistry of zircon crystals to their chronometric data with the

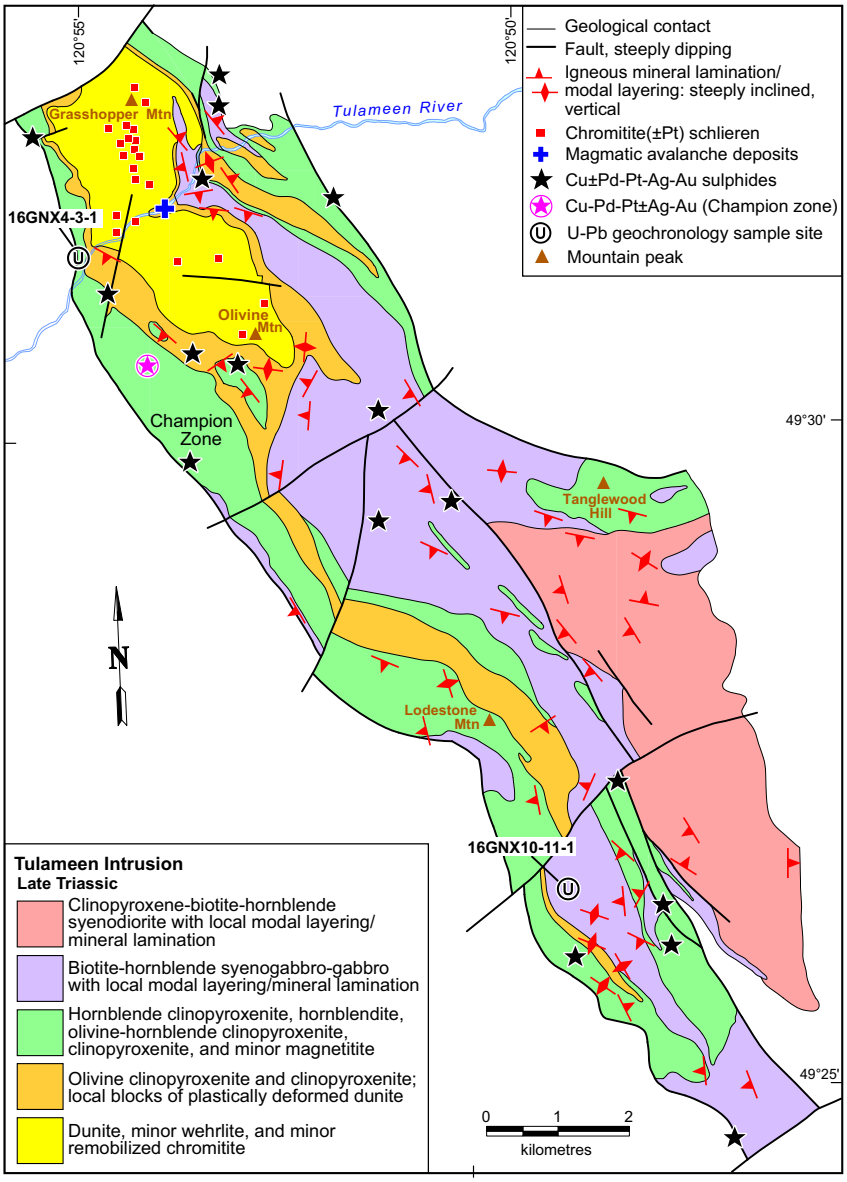

Figure 2. Generalized geological map of the Tulameen Alaskan-type intrusion, south-central British Columbia, showing chromitite (±PGE) localities in the dunite core (Nixon et al., 1997; Nixon, 2018) and Cu±PGE-Ag-Au sulphide occurrences, including the recently discovered Cu-Pd-Pt-rich Champion zone documented in this report. Abbreviation: Mtn = mountain.

goal of defining the specific conditions under which the analyzed zircon grains crystallized (Engi et al., 2017). Compared to our previous geochronological studies of convergent margin ultramafic-mafic intrusions in British Columbia (Giant Mascot intrusion: Manor et al., 2017; Turnagain intrusion: Nixon et al., 2020), the current study utilizes a workflow where the selection of zircon grains for high-precision CA-TIMS dating is determined by SEM-CL imaging and trace element compositions to ensure an internally consistent set of data from each analyzed zircon. From 20 geochronological samples representing major lithological units of the Tulameen intrusion, 11 yielded sufficient zircon grains for analysis. All analytical work is being conducted at the Pacific Centre for Isotopic and Geochemical Research at the University of British Columbia. Analytical techniques follow those described in detail in Scoates and Wall (2015), Ver Hoeve et al. (2018), and Wall et al. (2018).

The major accessory minerals in the Tulameen intrusion include zircon, apatite, and titanite. Euhedral apatite is present in most samples, whereas titanite is typically present in samples with no zircon. Titanite occurs in a variety of textural settings (e.g. wedge-shaped euhedral crystals, granular aggregates, rims around Fe-Ti oxides) and occurs in about 50% of the samples collected. Zircon from the Tulameen intrusion is characterized by a diverse range of internal structures under SEM-CL (Fig. 3). Herein we highlight the petrochronological attributes of two contrasting samples to demonstrate the potential for extracting information related to magmatic processes from the petrology, geochemistry, and geochronology of individual zircon grains. One is an ultramafic rock from the northwestern margin of the intrusion, adjacent to upper greenschist to lower amphibolite facies country rocks (biotite-hornblende clinopyroxenite, sample 16GNX4-3-1); the other is a monzodiorite from a gabbro-

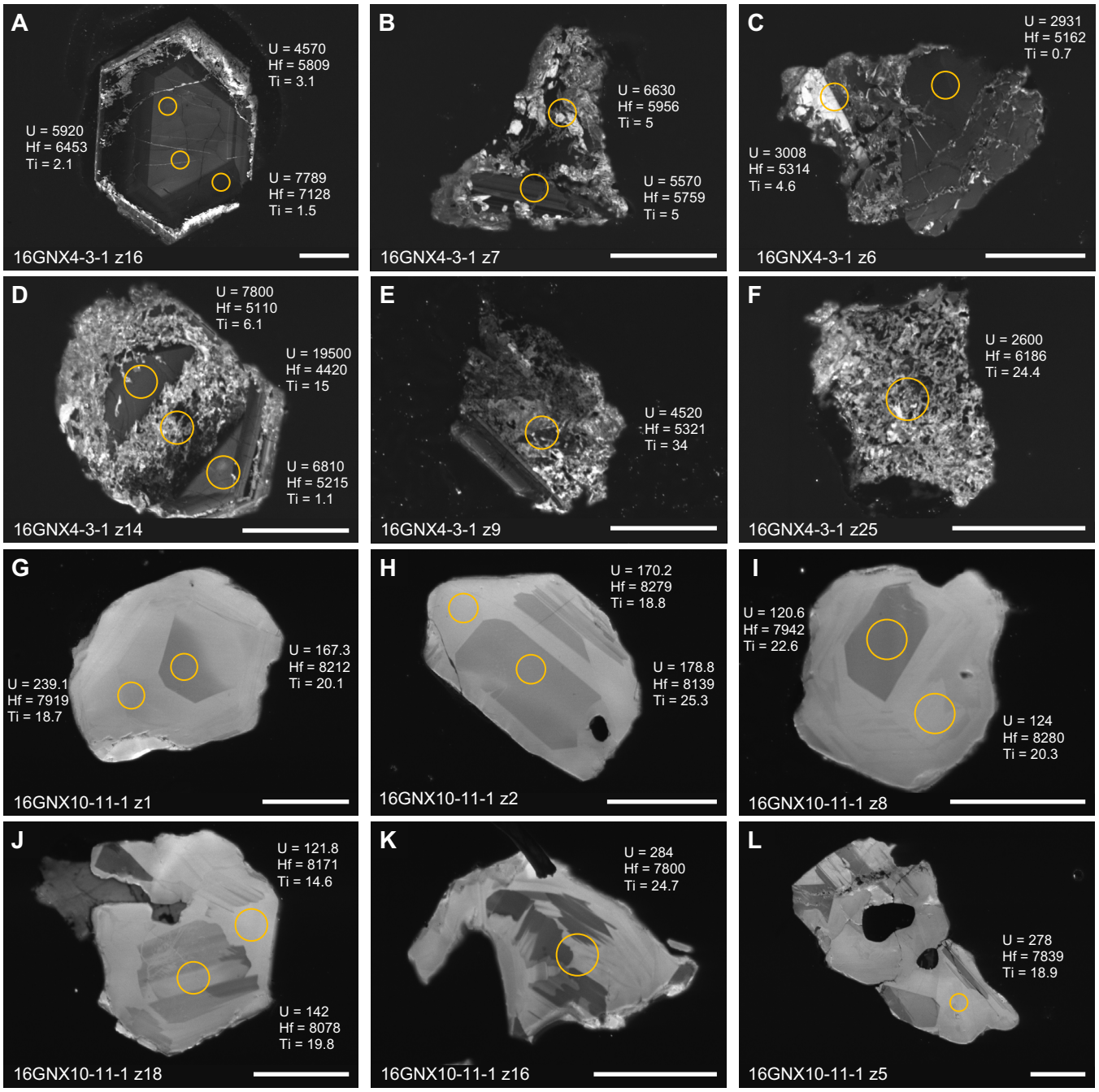

Figure 3. Scanning electron microscopy-cathodoluminescence (SEM-CL) images of zircon grains from representative samples of the Tulameen Alaskan-type intrusion. The circles indicate the locations of spot analysis by LA-ICP-MS (circle diameter is 34 µm). Values for U, Hf, and Ti (all in ppm) are shown adjacent to each spot. **a–f)** Zircon grains from sample 16GNX4-3-1 (biotite-hornblende clinopyroxenite). **g–l)** Zircon grains from sample 16GNX10-11-1 (monzodiorite). Note the presence of secondary and recrystallized CL-bright domains around and within the zircon grains from the clinopyroxenite sample compared to the essentially pristine zircon grains from the monzodiorite sample. Scales as indicated by the white bars (100 µm) on each photograph.

syenogabbro unit from the far southern end of the intrusion (monzodiorite, sample 16GNX10-11-1; Fig. 2). Zircon from the clinopyroxenite contains vestiges of oscillatory zoned magmatic zircon, generally with low CL response, that are enveloped or transected, or completely obliterated, by irregular and patchy domains and veins of CL-bright material (Fig. 3a-f). The domains and veins are interpreted to represent recrystallized and metamict (now strongly altered) zircon produced during deformation and associated metamorphism and hydrothermal activity (e.g. Scoates et al., 2017) that occurred after the Tulameen intrusion had solidified. In contrast, zircon from the monzodiorite is mostly pristine, showing only very minor effects of secondary processes along grain edges (CL-bright regions), and is dominated by simple zoning with CL-grey cores and

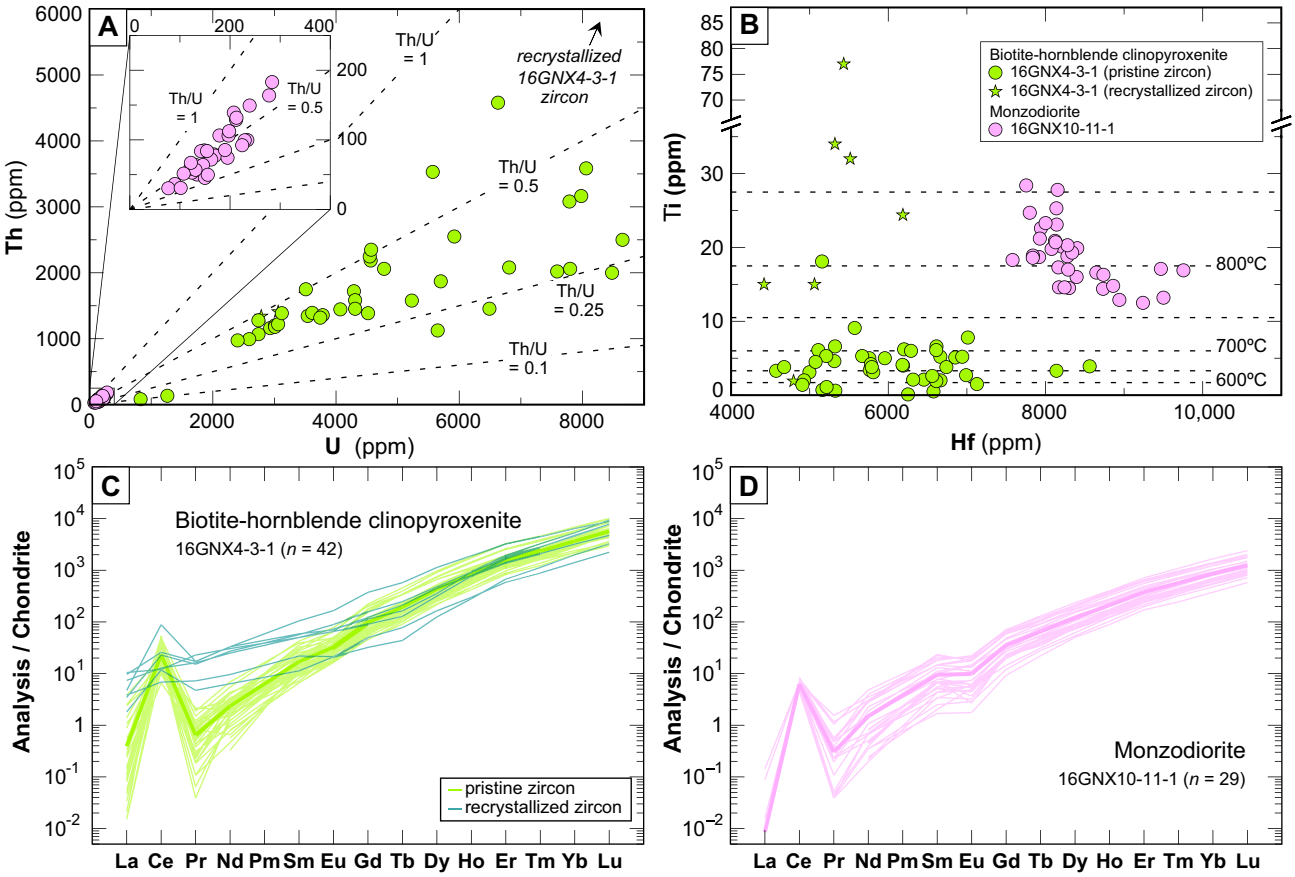

Figure 4. Trace element variations determined by LA-ICP-MS in zircon from representative samples of the Tulameen Alaskan-type intrusion. **a)** Plot of Th versus U with lines of constant Th/U indicated for reference. Anomalously high Th and U concentrations from the CL-bright recrystallized domains plot well off the scale of the graph. **b)** Plot of Ti versus Hf concentrations with horizontal dashed lines that are Ti-in-zircon temperatures calculated from Ferry and Watson (2007) using assumed a_{SiO_2} = 0.3 and a_{TiO_2} = 0.5 (i.e. no quartz or rutile are present in these samples; titanite is abundant). Note the break in scale on the Ti axis. Recrystallized zircon from the clinopyroxenite is indicated with the star symbol and is characterized by anomalously high Ti contents. **c)** Chondrite-normalized rare earth element (REE) patterns for zircon from sample 16GNX4-3-1 (biotite-hornblende clinopyroxenite). Patterns for CL-bright recrystallized zircon are shown in light blue and characterized by LREE enrichment. **d)** Chondrite-normalized rare earth element (REE) patterns for zircon from sample 16GNX10-11-1 (monzodiorite). Normalization values are from McDonough and Sun (1995).

broad CL-light rims (Fig. 3g-l). Inclusions of apatite occur in some zircon grains from the monzodiorite.

The geochemistry of zircon determined by LA-ICP-MS on mineral separates from the two samples is distinctive and highlights their different crystallization and post-crystallization histories (Fig. 4). Zircon from the clinopyroxenite has high but variable concentrations of U (850–8500 ppm) and Th (5–4500 ppm) with variable Th/U values (0.1–0.7; average = 0.4; Fig. 4a), consistent with derivation from an extremely fractionated interstitial melt. In contrast, zircon from the monzodiorite has relatively low and restricted concentrations of U and Th (U = 80–290 ppm; Th = 25–190 ppm; Th/U ≈ 0.5). Zircon from the two different rock types shows distinctive Ti-Hf systematics where Ti is a monitor of temperature (Ferry and Watson, 2007) and Hf is a proxy for the extent of fractionation (Grimes et al., 2009; Ver Hoeve et al., 2018; Fig. 4b). In the clinopyroxenite, zircon defines a nearly horizontal Ti-Hf trend with a limited range of very low Ti concentrations, and a wide range of Hf concentrations (4500–8500 ppm), a feature taken to indicate crystallization at near-solidus conditions. Anomalously high Ti contents (15–80 ppm) correlate with analyses of recrystallized, CL-bright zircon (Fig. 4b), indicating the addition of Ti to the magmatic zircon during secondary processes. In contrast, zircon from the monzodiorite defines the typical curvilinear Ti-Hf relationship that indicates the crystallization of zircon from a melt undergoing progressive fractionation (i.e. increasing Hf) during cooling (i.e. decreasing Ti; Fig. 4b). Estimates of crystallization temperatures based on Ti-in-zircon thermometry (Ferry and Watson, 2007) are cooler (average = 650ºC) for zircon from the clinopyroxenite compared to zircon from the monzodiorite (850–760°C). This confirms the near-solidus crystallization of zircon in the ultramafic rock relative to the higher temperatures of zircon crystallization as a liquidus phase in the monzodiorite; a similar

relationship was observed for zircon from ultramafic and dioritic rocks in the Giant Mascot and Spuzzum intrusions of southwestern British Columbia (Manor et al., 2017). Chondrite-normalized rare earth element (REE) patterns of zircon from the two samples from the Tulameen intrusion display typical igneous zircon patterns with relatively depleted light REE (LREE) and relatively enriched heavy REE, strong positive Ce anomalies (most significant in the clinopyroxenite), and subtle negative Eu anomalies (more negative in the monzodiorite; Fig. 4c,d). Zones of recrystallized zircon from the clinopyroxenite are characterized by anomalously flat LREE patterns indicating the addition of LREE during secondary processes. Overall, the absolute abundances of REE are higher, and REE profiles are more fractionated (i.e., higher Lu/Nd values) in zircon from the clinopyroxenite, compared to zircon from the monzodiorite (Fig. 4c,d).

The CA-ID-TIMS U-Pb zircon geochronology from the Tulameen intrusion reveals a range of $^{206}Pb/^{238}U$ dates for each sample at ca. 204–205 Ma (Fig. 5). The ability to date individual zircon crystals, or fragments of grains, to high precision by CA-ID-TIMS now systematically reveals dispersed zircon dates where it is no longer adequate to simply calculate weighted mean dates from a population, typically the oldest, and use them to infer crystallization ages (e.g. Samperton et al., 2015; Manor et al., 2017). The chemical abrasion technique (CA-ID-TIMS) of Mattinson (2005) allows for the removal of zircon domains that have lost Pb from the interior of grains and for the subsequent analysis of low-U+Th, closed-system residues with concordant results and ages with significantly improved accuracy. The U-Pb results for analyses completed to date for both samples are concordant to slightly normally and reversely discordant and they span a range of $^{206}Pb/^{238}U$ dates from 205.36 ± 0.28 Ma to 204.79 ± 0.24 Ma (Δt ≈ 0.57 Ma) for the clinopyroxenite (n = 5) and from 205.01 ± 0.29 Ma to 203.36 ± 0.72 Ma (Δt ≈ 1.74 Ma) for the monzodiorite (n = 8; Fig. 5). A single zircon from the monzodiorite yields an anomalously young concordant date of 178.26 ± 1.03 Ma (not shown in Fig. 5), reflecting the effects of Pb loss since crystallization, not mitigated by chemical abrasion pretreatment. The dispersion in the dates of both samples is provisionally attributed to protracted, autocrystic zircon crystallization following the approach outlined by Samperton et al. (2015), where autocryst refers to zircon associated exclusively with a distinct pulse or increment of magma (Miller et al., 2007). Except for recrystallized zircon in the clinopyroxenite, both samples contain what appear to be single populations of autocrystic zircon grains with relatively simple internal structures, no growth discontinuities or cores, and coherent trace element variations.

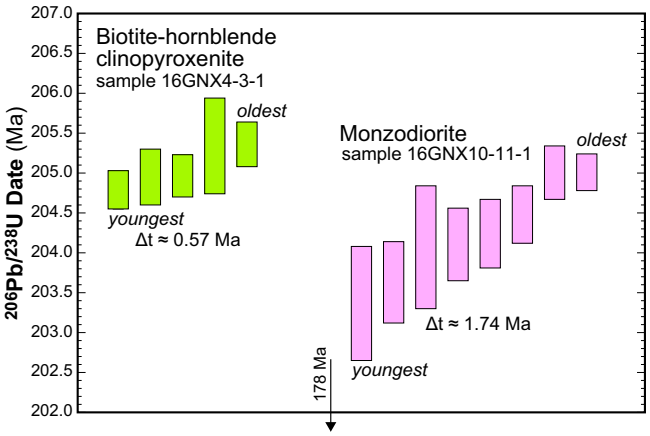

Figure 5. Preliminary chemical abrasion-isotope dilution-thermal ionization mass spectrometry (CA-ID-TIMS) U-Pb zircon geochronological results from the Tulameen Alaskan-type intrusion presented as rank-order plots of $^{206}Pb/^{238}U$ dates for sample 16GNX4-3-1 (biotite-hornblende clinopyroxenite) and for sample 16GNX10-11-1 (monzodiorite). Each bar represents the result of the analysis of a single zircon grain or fragment; the height of the bar corresponds to the 2σ uncertainty. Both samples show a range of $^{206}Pb/^{238}U$ dates at ca. 204–205 Ma. This dispersion (Δt) is provisionally attributed to protracted autocrystic zircon crystallization in the magmas that crystallized to produce clinopyroxenite and monzodiorite. Note that a single analysis from the monzodiorite with a much younger $^{206}Pb/^{238}U$ date of ca. 178 Ma is off the scale of the plot and is attributed to Pb loss since crystallization.

The preliminary U-Pb geochronological results indicate emplacement and crystallization of the Tulameen Alaskan-type ultramafic-mafic intrusion over a relatively restricted interval of time (204–205 Ma) in the Late Triassic. It is increasingly recognized that many plutonic rocks, spanning the spectrum of compositions from mafic to felsic, were emplaced into the middle to upper crust incrementally through the amalgamation of smaller volume batches in the form of horizontal sheets or sills (e.g. Matzel et al., 2006; Schoene et al., 2012; Annen et al., 2015; Wall et al., 2018). In British Columbia, the geochronology of composite ultramafic-mafic intrusions now demonstrates a range of emplacement and crystallization timescales, from relatively short (ca. 93 Ma for the Giant Mascot intrusion: Manor et al., 2017; ca. 204–205 Ma for Tulameen: this study) to extended (ca. 185–189 Ma for Turnagain: Nixon et al., 2020). These ultramafic-mafic intrusions represent the crystallized products of magmatic systems in arc environments where individual arcs may be active for prolonged periods of up to several million years, but may also be episodic with discrete periods of enhanced magmatism separated by lulls during which magma productivity is significantly reduced (e.g. DeCelles et al., 2009; Gehrels et al., 2009; Paterson and Ducea, 2015). The new dates for the Tulameen intrusion are also coincident with a 6 million year magmatic flare-up centred on 205 Ma in the Stikine and Quesnel arcs

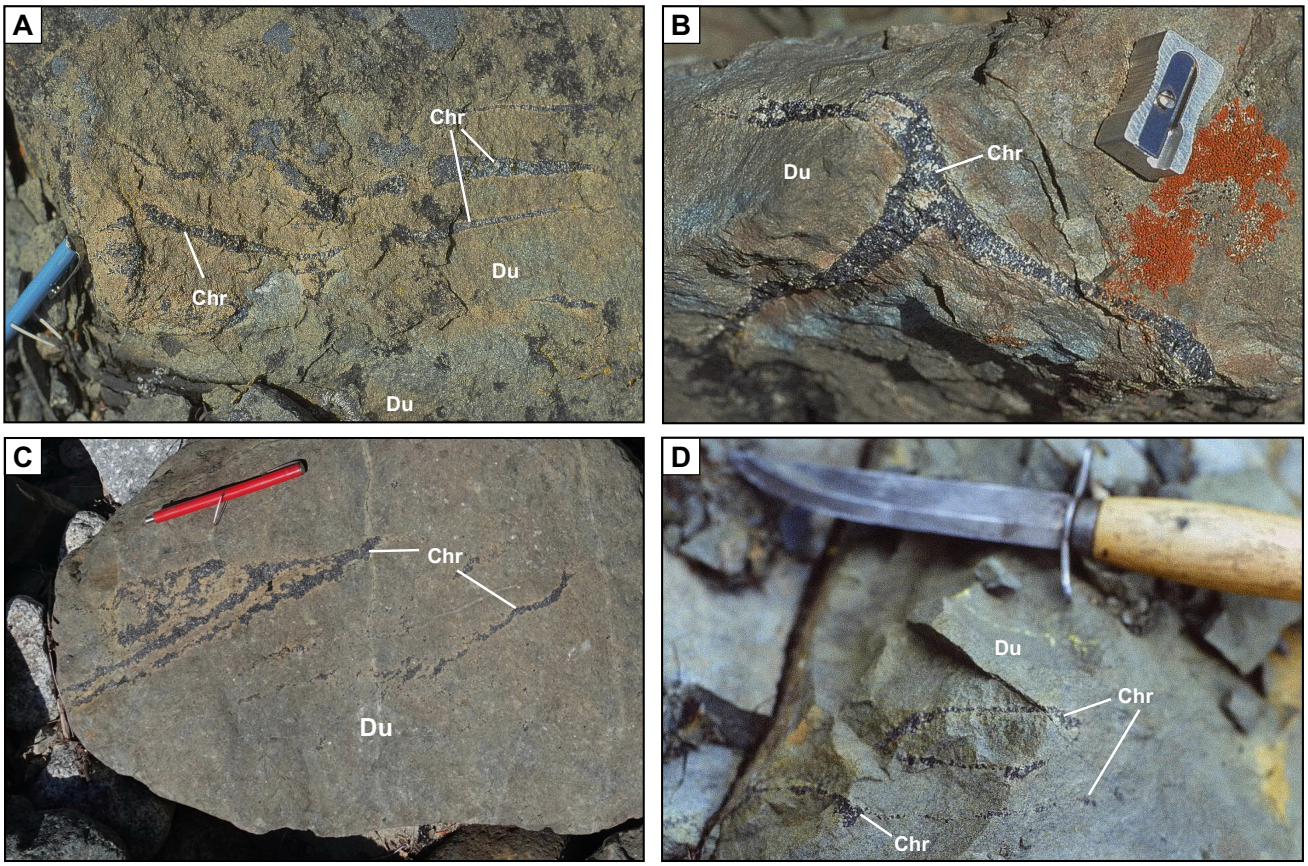

Figure 6. Photographs showing remobilized chromitites in the dunite core of the Tulameen intrusion. **a)** Massive chromitite schlieren (Chr) in dunite (Du) showing typical curvilinear morphology. The visible part of the pencil magnet is 6 cm in length. **b)** Contorted "wishbone" chromitite in dunite. The pencil sharpener is 3 cm in length. **c)** Layered chromitite-dunite inclusion and fine stringers of chromitite in a loose boulder of dunite at the confluence of Britton Creek with the Tulameen River. The pencil magnet is 13 cm in length. **d)** Circular chromitite body proximal to a fine seam of chromitite that shows no evidence of such deformation. The visible part of knife is 20 cm in length.

(Logan and Mihalynuk, 2014). During this time, more than 90% of the known copper endowment of the Stikine and Quesnel arc terranes was produced, resulting in the most prolific Cu-Au porphyry mineralization epoch in British Columbia. Enhanced magmatic activity at this time has been related to stalled subduction, arc-parallel tearing of the subducting slab that lead to early (ca. 210 Ma) production of picritic magmas followed by lower degree partial melts parental to the alkalic Cu-Au porphyries (Logan and Mihalynuk, 2014). The geochronological results from the Tulameen intrusion suggest a direct petrogenetic relationship between Alaskan-type ultramafic-mafic intrusions, the cumulate products of hydrous primitive mantle-derived arc magmas (e.g. up to Fo_{92} olivine at Tulameen: Nixon et al., 1990; Rublee, 1994; and Turnagain, Scheel, 2007), and the formation of Late Triassic Cu-Au porphyry deposits within the northern Cordilleran Stikine-Quesnel arc systems.

Chromitite

Chromitites in the dunite core of the Tulameen intrusion have attracted exploration interest in the past during the search for the origin of historic platinum-rich placers in the Tulameen River. The global platinum exploration boom in the mid-1980s lead to activity primarily focused on Grasshopper Mountain, and later research established platiniferous chromitites in bedrock as the source of platinum in the placers (Nixon et al., 1990). The dunite core of the Tulameen intrusion hosts chromitites with Pt abundances of up to 9.3 g/t Pt and high Pt/Pd values (~127: Nixon et al., 1990). The platinum group minerals are predominantly Pt-Fe alloys that crystallized directly from parental melts in equilibrium with chromite and laurite in a low-fS_2 environment (Nixon et al., 1990; Brenan and Andrews, 2001).

The features exhibited by chromitites in Tulameen dunite (Fig. 6) appear common to other Alaskan-type bodies in British Columbia and elsewhere (e.g. Nixon et al., 1997; Anikina et al., 2014). Chromitites are confined to the dunite core (Fig. 2), and their distribution, as mapped, is more a function of the time spent scouring the more easily accessible outcrops than their true spatial distribution within the dunite. The chromitites

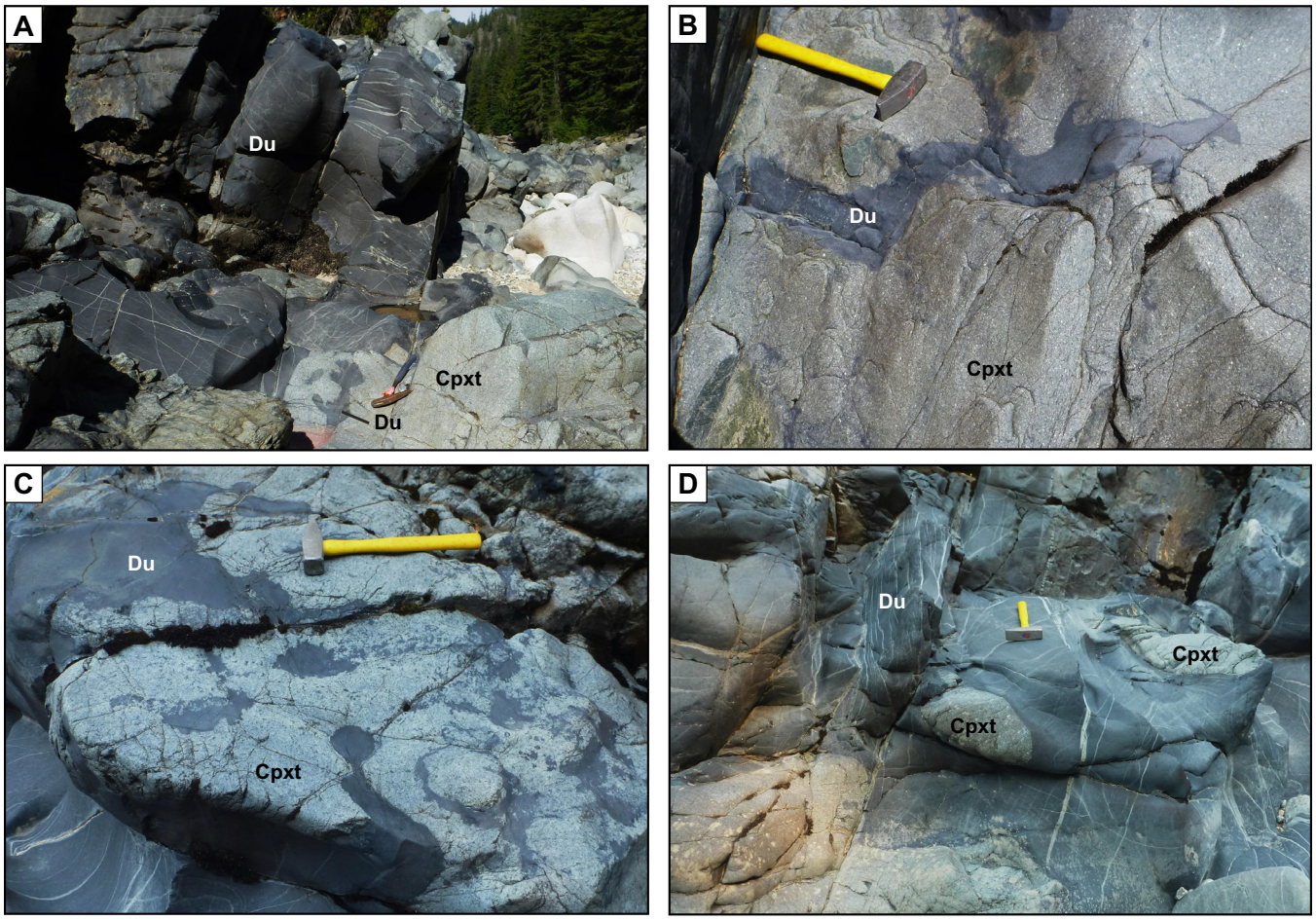

Figure 7. Photographs showing inclusions of dunite in 'magmatic avalanche' deposits exposed in the Tulameen River bed at the eastern periphery of the dunite core. **a)** A large (15 m across) block of dunite (Du) showing irregular contacts with olivine clinopyroxenite/clinopyroxenite (Cpxt) and intricately shaped dunite inclusions in adjacent clinopyroxenite. **b)** Elongate inclusion of dunite in clinopyroxenite exhibiting small protrusions into its host (right end of the dunite). **c)** Bulbous, ragged, and finely disaggregated inclusions of dunite in clinopyroxenite. Note the preferred orientation of dunite disaggregation trails (parallel to the hammer) and a round inclusion of clinopyroxenite (lower right) that has been almost completely exhumed from the dunite. **d)** Rounded inclusions of clinopyroxenite in a dunite pod. Note the highly crenulated and disaggregated dunite-clinopyroxenite contact at the bottom of the photograph. Hammers for scale are 37 cm in length.

generally occur as massive schlieren that reach over a metre in length, however, they are commonly less than 30 cm long by 4 cm wide (Fig. 6a). There is ample evidence for disruption and ductile deformation of formerly layered chromitite-dunite sequences, and some deformed chromitites defy a simple in situ structural explanation for their geometry (Fig. 6b,d). Rare inclusions of layered chromitites attest to the origin of the more common isolated chromitite schlieren (Fig. 6c). These features provide evidence for ductile disaggregation, transport, and redeposition of hot, malleable chromitite-olivine cumulates during crystallization of the dunite core. Similar features in chromitites of the Polaris intrusion are described below.

Magmatic Avalanche Deposits

Remobilized dunite-clinopyroxenite cumulates, herein interpreted as 'magmatic avalanche' deposits, are well exposed at the eastern margin of the dunite core along a 400 m stretch of the Tulameen River bed (Fig. 2). The deposits comprise dunite inclusions, up to 15 m across, immersed in an olivine clinopyroxenite/clinopyroxenite unit in sheared contact with variably serpentinized dunite. Displacement on this contact does not appear to be significant.

The dunite inclusions are generally weakly serpentinized and exhibit some unique features. The largest block of dunite has irregular contacts with the host clinopyroxenite; the latter contains dunite inclusions with intricate shapes that may have spalled off the neighbouring large dunite block (Fig. 7a). Some dunite inclusions are distinctly elongate and exhibit relatively smooth contacts with their clinopyroxenite host except for a few small protuberances (Fig. 7b). Locally, the dunite inclusions show smooth bulbous, as well as ragged morphologies with crenulated margins that dissipate into elongate trains of cm- to mm-size crystal clots dispersed in the clinopyroxenite matrix. The pre-

ferred orientation of these clots likely formed during deposition (Fig. 7c). Bulbous protrusions of dunite in clinopyroxenite and inclusions of clinopyroxenite in dunite are also evident (Fig. 7d) and provide evidence for the viscous intermingling of cumulates during crystallization of the host clinopyroxenite. These processes also appear to be operating in the chaotically intermingled units at Polaris (described below).

Champion Zone: Cu-PGE Mineralization

The Champion zone is a 700 m long zone of intermittent Cu-sulphide mineralization exposed near the western margin of the Tulameen intrusion along a logging road overlooking Champion Creek, for which the showing is named (Fig. 2). The mineralization is hosted in magnetite-hornblende±biotite clinopyroxenite and hornblendite with minor, thin (several cm) horizons of magnetitite. Textural evidence in the least altered rocks indicates that the mineralization is magmatic in origin; however, a metamorphic overprint is evident locally as are restricted zones of intense pyritic hydrothermal alteration. Scattered occurrences of Cu±Ag-Au-PGE mineralization are hosted by ultramafic and gabbroic rocks in other parts of the intrusion (Fig. 2) and may have similar origins as the Champion zone sulphides described below.

Cu sulphides (trace to 2 vol.%) are sparsely distributed throughout the Champion zone and are practically invisible in outcrop, except where weak malachite staining betrays their presence. The primary sulphide minerals are chalcopyrite and lesser bornite accompanied by minor covellite, digenite/chalcocite, and rare pyrrhotite. Pyrite is locally abundant as a hydrothermal overprint replacing magmatic sulphides (mainly chalcopyrite). Four principal textural groupings of sulphide minerals are recognized: 1) inclusions (mostly <30 μm across but reaching 60 μm in diameter) hosted by silicates (clinopyroxene, amphibole) and oxide (magnetite) (Fig. 8a); 2) primary sulphides that occur interstitially within the cumulate framework (Fig. 8b); 3) interstitial sulphides recrystallized and intergrown with metamorphic minerals (Fig. 8c); and 4) secondary Fe sulphides that replace primary Cu-sulphide minerals (Fig. 8d).

Inclusions of chalcopyrite, bornite, minor pyrite, and rare pyrrhotite are found in unaltered silicates and oxides (Fig. 8a). Chalcopyrite commonly forms inclusions in hornblende, clinopyroxene, and magnetite; rare pyrrhotite is confined to inclusions in clinopyroxene where it coexists with chalcopyrite. Bornite occurs in hornblende and magnetite and may be accompanied by chalcopyrite; bornite has not been observed to coexist with pyrrhotite.

Interstitial chalcopyrite and bornite occur as primary sulphides adjacent to unaltered cumulus clinopyroxene and cumulus or postcumulus hornblende and magnetite. Internal features commonly observed in the sulphides include crystallographically controlled, fine exsolution lamellae of chalcopyrite in bornite, and vermicular intergrowths of bornite and chalcopyrite (Fig. 8b). The sulphides locally display alteration rims of covellite and digenite/chalcocite, possibly developed during metamorphism. Malachite and Fe-oxide/hydroxide rims on sulphides are locally well developed as a result of weathering.

Recrystallized interstitial sulphides, predominantly chalcopyrite, are locally intergrown with actinolite, epidote, chlorite, and secondary titanite (Fig. 8c). Sulphide morphologies are typically angular due to control by secondary silicate grain boundaries. Locally, sulphides are remobilized along microfractures and cleavage planes of primary silicates. These textures are attributed to recrystallization and partial replacement of sulphides at upper greenschist-facies conditions, promoted by localized penetration of circulating metamorphic fluids along grain boundaries.

Late-stage hydrothermal pyrite locally occupies fractures and veinlets, and forms narrow (metre-scale) zones of more pervasive replacement of primary interstitial sulphides (Fig. 8d). These zones are typically steeply dipping and appear to crosscut the general trend of the Cu-sulphide mineralization. Rarely, the more pervasive hydrothermal assemblages involve pyrite, chalcopyrite, and pyrrhotite replacing primary silicate minerals.

In addition to the base-metal sulphides, platinum group minerals (PGM) identified in the Champion zone include mertieite (Pd_8Sb_3), sperrylite ($PtAs_2$), and an unknown Pd-Sb-telluride phase that may be a mixture of mertieite and a Pd-telluride (e.g. kotulskite or keithconnite). The PGM form small discrete grains (<7 μm) that are mainly distributed among secondary minerals (chlorite, actinolite, titanite rims on magnetite), except for the Pd-Sb-Te phase(s), which is enclosed in chalcopyrite. These observations suggest that the PGM were remobilized during metamorphism.

Preliminary geochemical results for bulk-rock samples from the Champion zone with low amounts (<2 vol.%) of sulphides yield up to 5200 ppm Cu, 1.15 ppm Pd, 0.79 ppm Pt, and 531 ppb Au with Pd/Pt ≈ 1.5. The abundance of sulphur is consistently low (<530 ppm) throughout the zone. The Cu-rich nature of the sulphides and their low modal proportions, the depletion in sulphur and relative enrichment in Pd, are attributes of Cu-PGE mineralization documented in stratiform or 'reef-style' mineralization in tholeiitic layered intrusions.

The mineralogical and geochemical traits of mineralization in the Champion zone and selected layered intrusions are compared in Table 1. The layered intru-

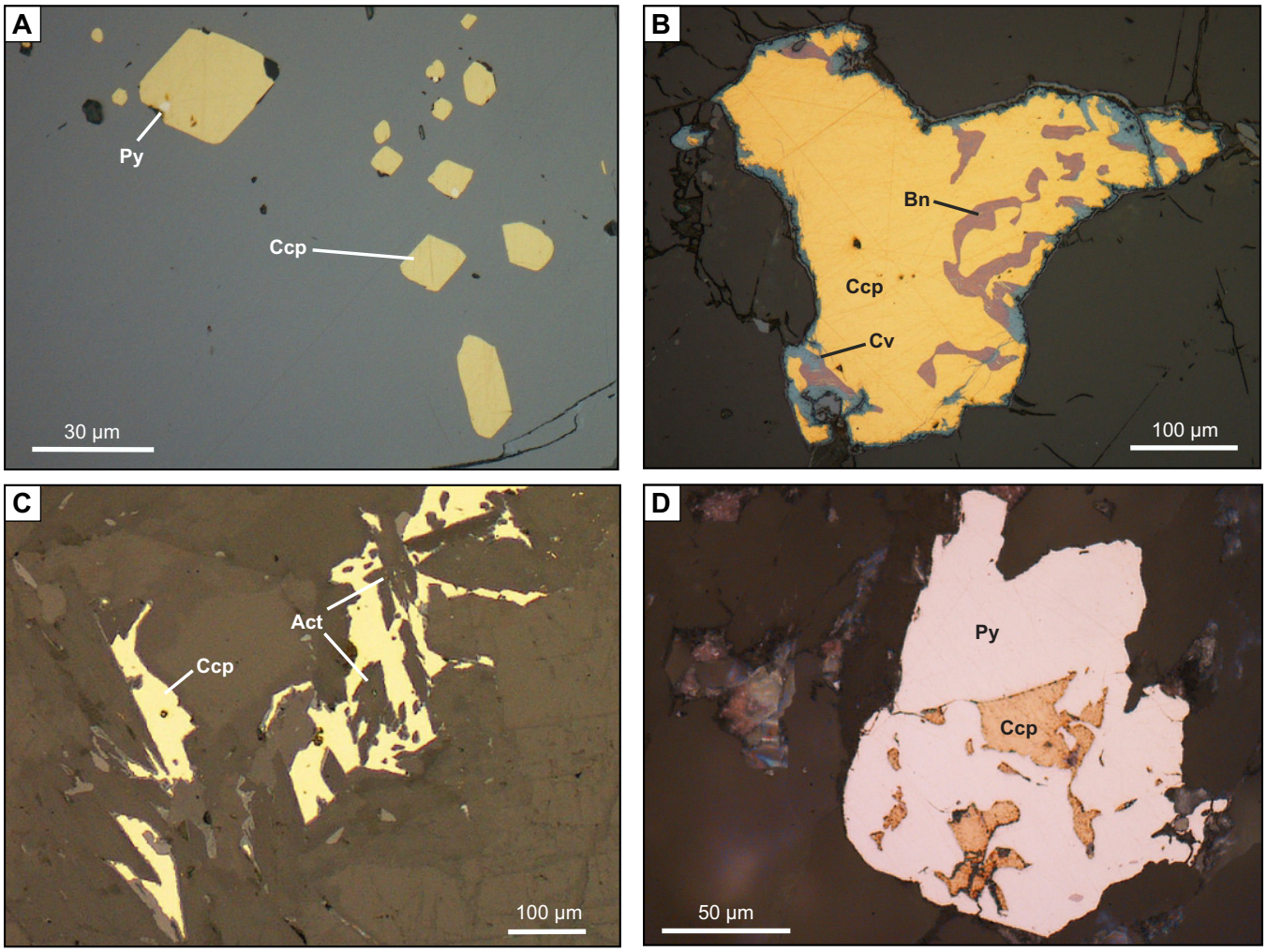

Figure 8. Reflected light photomicrographs showing textural features exhibited by Cu sulphides in ultramafic rocks of the Champion zone. **a)** Chalcopyrite inclusions (Ccp) displaying negative crystal shapes with minor inclusions of pyrite (Py) in cumulus magnetite (magnetite-hornblende clinopyroxenite, sample 16GNX15-7-3). **b)** Interstitial chalcopyrite (Ccp) with vermicular inclusions of bornite (Bn) and partly altered to covellite (Cv). Note the minor chalcopyrite exsolution lamellae that are barely visible in the bornite (magnetite-hornblende clinopyroxenite, sample 17GNX20-3-7). **c)** Recrystallized interstitial chalcopyrite (Ccp) partly replaced by/intergrown with actinolite (Act) (magnetite-hornblende clinopyroxenite, sample 17GNX20-7-1). **d)** Hydrothermal pyrite (Py) replacing interstitial chalcopyrite (Ccp) preserved as irregular relict grains (biotite-hornblende-magnetite clinopyroxenite, sample 17GNX20-12-1). Scales as noted on each photograph.

sions are considered to represent crystallization in closed systems, except for Rincón del Tigre in Bolivia, which has been interpreted as a periodically replenished open-system (Prendergast, 2000), and the W Horizon in the Marathon deposit, Ontario, where spectacular grades may reflect metal upgrading of sulphides via magma flow in conduits (Ames et al., 2017; Good et al., 2017). Remarkable PGE grades (Pt+Pd = 15 g/t, Table 1) are also documented in a 1 metre thick magnetite layer in the Stella intrusion, South Africa (Maier et al., 2003). In the Skaergaard intrusion in Greenland, one of the most intensively studied layered intrusions in the world, the Platinova Reef has an estimated (subeconomic) resource of 23 Mt at 2.3 g/t Au, 0.7 g/t Pd, and 0.1 g/t Pt (contained metal 1.7 Moz Au, 0.5 Moz Pd, and 0.04 Moz Pt) at a cut-off grade of 1.5 g/t equivalent Au (Holwell and Keays, 2014; Holwell et al., 2015).

The Cu-PGE stratiform mineralization is commonly associated with evolved, Fe-Ti oxide-rich gabbro or ferrogabbro cumulates that occur high in the stratigraphy after crystallization of two-thirds or more of the parental magma. Chalcopyrite and/or bornite generally account for the very low amount (<0.2 vol.%) of sulphide typically present in the reefs along with minor digenite, covellite, and chalcocite (Table 1). However, base-metal sulphides are commonly not the most important hosts for PGE but rather discrete platinum group minerals (PGM) such as alloys, PGE-rich sulphides, bismuthides, arsenides, tellurides, and bismuthotellurides (e.g. Godel, 2015).

In comparison to layered intrusions, Cu-rich sulphide mineralization in the Champion zone occurs in evolved ultramafic rocks (magnetite-rich hornblende

Table 1. Cu-PGE reefs in layered intrusions versus Tulameen Alaskan-type intrusion (Champion zone).

Name	Age	Sulphides		Maximum (ppm)						Host rock	Oxide	Ref.
	(Ma)	Type	vol.%	S	Cu	Pd	Pt	Au	Pd/Pt		(vol.%)	
Stella, South Africa	3033	Ccp, Py	m	1150	1096	7.6	7.3	0.67	~1	magt	>50	1
Nuasahi, India	3100	Ccp, Cc, Cv	tr–m	bdl	826	3.8	0.24	0.358	15.8	magt	70	2
PMZ, Sonju Lake, USA	1096	Ccp (Bn)	<0.2	400	<200	1	0.1	0.085	10	Fe-Ti-oxide gabbro	≤12	3, 4, 5
Marathon W Horizon, Coldwell, ON	1105–1108	Ccp, Bn (rare Pn, Po, Py, Mi, Cbt)	1–5	<1 (wt%)	5613	42.2*	8.9*	2.4	4.7*	gabbro		6, 7
PMZ, Rincon del Tigre, Bolivia	990	Ccp, Bn, Cc, Cv (Py, rare Po, Pn)	tr–m	nd	~100	1.8	0.68	0.35	2.6	Mag gabbro	5–30	8
Platinova Reef (Pd zone), Skaergaard, Greenland	56	Bn, Dg (Ccp)	<0.1	<100	300	4	0.2	0.3	20	oxide-rich gabbro	10–40	9, 10, 11
Champion Zone, Tulameen, BC	ca. 204–205	Ccp, Bn, Cv, Dg, Py (rare Po)	tr–2	530	5200	1.15	0.79	0.531	~1.5	Mag-Hbl cpxite; Mag hbt (magt)	5–50	this study

*Conservative values, maximum abundances reported: 67 ppm Pd and 39 ppm Pt (Pd/Pt = 1.7) over 2 m.

Abbreviations: bdl = below detection limit, Bn = bornite, Cbt = colbaltite, Cc = chalcocite, Ccp = chalcopyrite, cpxite = clinopyroxenite, Cv = covellite, Dg = digenite, Hbl = hornblende, hbt = hornblendite, m = minor, Mag = magnetite, magt = magnetitite, Mi = millerite, PMZ = precious-metal zone, Pn = pentlandite, Po = pyrrhotite, Py = pyrite, Ref. = reference, tr = trace, vol.% = volume percent.

References: 1) Maier et al., 2003; 2) Prichard et al., 2018; 3) Miller, 1999; 4) Li et al., 2008; 5) Miller and Ripley, 1996; 6) Good et al., 2017; 7) Ames et al., 2017; 8) Prendergast, 2000; 9) Holwell and Keays, 2014; 10) Holwell et al., 2015; 11) Godel et al., 2014.

clinopyroxenites and hornblendites) at the zoned margin of the intrusion. The Ni-poor nature of magmatic sulphides at Tulameen may be explained by early depletion of Ni by olivine fractionation in silicate melts prior to the onset of sulphide liquid immiscibility. The timing of sulphide saturation in fractionating silicate melts is dependent on a number of factors, some of which appear to have ramifications for sulphide mineralization at Tulameen. Fractional crystallization combined with progressive magmatic oxidation, at oxygen fugacities extending through the sulphide-sulphate transition (Jugo et al., 2010), results in equilibrium sulphide melts with increasingly higher Cu/Fe ratios (Wohlgemuth-Ueberwasser et al., 2013). Under these conditions, and where sulphide saturation of a silicate melt is delayed, the first equilibrium sulphide melts to form are expected to be Cu-rich, leading to bornite and/or chalcocite crystallization (Wohlgemuth-Ueberwasser et al., 2013). Fractionation of magnetite would serve to reduce the FeO content, Fe^{3+}/Fe^{2+}, fO_2 and SO_4^{2-}/S^{2-} of a silicate melt, all effects that would bring the melt closer to sulphide saturation (e.g. Haughton et al., 1974; Jenner et al., 2010; Keays and Tegner, 2015). Degassing of hydrous magmas in shallow crustal reservoirs would also drive the melt towards sulphide saturation (Fortin et al., 2015). Further mineralogical and geochemical studies are needed to resolve which of these and other factors are critical to the origin and timing of Cu-PGE mineralization at Tulameen and other Alaskan-type intrusions in hydrous and oxidizing supra-subduction zone settings.

POLARIS INTRUSION

The Early Jurassic Polaris ultramafic-mafic intrusion (45 km^2) in north-central British Columbia (Fig. 1) is one of the best exposed Alaskan-type intrusions in the North American Cordillera, and second in size only to Tulameen. The Polaris intrusion is a westerly dipping (30–50°) sill-like body (Nixon et al., 1997; Nott et al., 2020) emplaced into Late Paleozoic metasedimentary and metavolcanic rocks of the Lay Range assemblage (Fig. 9). The host rocks of the Lay Range assemblage (Mississippian-Permian: Ferri, 1997) are correlative with the Harper Ranch subterrane in southern British Columbia, and they form the substrate for the composite Middle Triassic-Early Jurassic volcanic arc that forms the bulk of Quesnel terrane. Emplacement of the Polaris intrusion into the Quesnel terrane (ca. 186 Ma: Nixon et al., 2019) was coeval with emplacement of the Turnagain Alaskan-type intrusion in the Yukon-Tanana terrane (ca. 189–185 Ma: Nixon et al., 2020), and marks the initial accretion of peri-Laurentian arc terranes to the western continental margin of ancestral North America in the Early Jurassic (Nelson et al., 2013; Monger and Gibson, 2019; Nixon et al., 2020).

Internal Zonation

The Polaris intrusion is composed of adcumulate to heteradcumulate (clinopyroxene-bearing) dunite(-chromitite), wehrlite, olivine clinopyroxenite, clinopyroxenite, hornblende clinopyroxenite, hornblendite, and gabbro-diorite (Fig. 9; Nott et al., 2020). Hornblende clinopyroxenite and gabbro-diorite contain accessory (<2 vol.%) apatite, titanite, and zircon. Minor amounts of disseminated orthomagmatic sulphides are found locally in clinopyroxene- and hornblende-rich rocks.

Along the eastern thrust margin of the Polaris intrusion, a narrow belt of ultramafic cumulates is preserved locally and passes gradationally (east to west) from olivine clinopyroxenite, through wehrlite and olivine

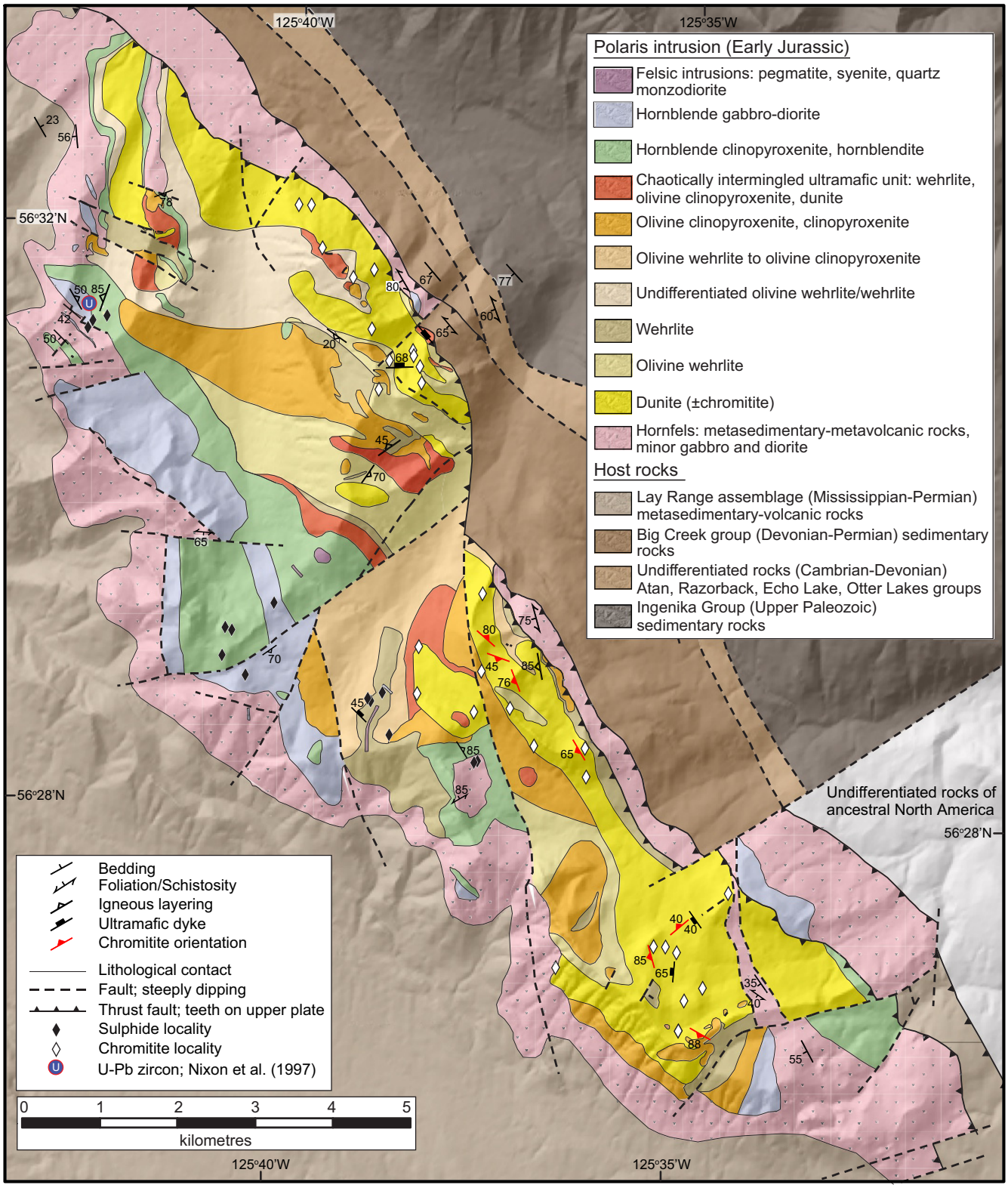

Figure 9. Generalized geological map of the Polaris Alaskan-type ultramafic-mafic intrusion showing regional geology, contact relationships, and chromitite and magmatic sulphide localities (*modified from* Nixon et al., 1997; and Nott et al., 2020).

wehrlite into dunite (Fig. 9). This zonation may have developed at the intrusive contact with the Lay Range assemblage, which has been removed by faulting. The overall internal distribution of rock types in the Polaris intrusion shows the opposite sense of zonation, with ultramafic rocks predominant in the eastern part of the intrusion and the more evolved feldspathic and hornblende-rich rocks concentrated in the west (Fig. 9). This

intrusion-scale distribution of ultramafic-mafic rock types appears to represent a crude internal stratigraphy that has been disrupted locally by faulting and zones of chaotically intermingled cumulates (discussed below).

Contact Relationships

Despite the disruption by syn- to post-emplacement ductile and brittle faulting (Fig. 9), igneous contacts between the mafic-ultramafic rock types of the Polaris intrusion are generally well preserved (Fig. 10). Where primary lithological zonation is exposed, most commonly at the transition from dunite through wehrlite to olivine clinopyroxenite, regular and continuous lithological contacts are gradational on the metre-scale (Fig. 10a). The more evolved, hornblende-rich and feldspathic rocks are typically heterogeneous on both hand- and outcrop-scale (Fig. 10h). Some igneous contacts between mafic and ultramafic rocks are intrusive and marked by what are interpreted as partially cannibalized enclaves of clinopyroxenite in a gabbro-diorite matrix.

Chaotically Intermingled Cumulates

Chaotically intermingled ultramafic cumulates on decametre- to metre-scale are a prominent feature in parts of the Polaris intrusion, especially near the margins of clinopyroxenite and wehrlite units, and less commonly dunite (Fig. 9). Contacts between intermingled rock types are commonly irregular and vary from sharp to gradational or diffuse. Dykes of coarse-grained to pegmatitic olivine clinopyroxenite/clinopyroxenite cut dunite and wehrlite, and foliated planar dykes of dunite or olivine wehrlite to wehrlite locally cut olivine clinopyroxenite (Fig. 10b–e). Local dense swarms of olivine clinopyroxenite/clinopyroxenite dykes with centimetre-scale offshoots cut dunite and olivine wehrlite. Centimetre- to metre-scale irregular, patchy, clinopyroxenite pods and dykes that have gradational to diffuse contacts with olivine-rich wallrocks may indicate reactive replacement of dunite/olivine wehrlite cumulates by clinopyroxene-rich magmas. The intermingled zones also contain fragmental cumulates, some composed of subrounded dunite-wehrlite clasts in sharp to diffuse contact with a clinopyroxene-rich host, whereas others comprise tabular blocks of wehrlite with a pronounced foliation set in a similar matrix (Fig. 10f,g).

The textural and ambivalent intrusive relationships in the chaotically intermingled units indicate both ductile and brittle behaviour of ultramafic cumulates involved in the mingling and intrusive activity. Ductile behaviour is apparent in the highly irregular, sharp to diffuse contacts and necking features observed among ultramafic rock types (Fig. 10b,e). Injection of dunite dykes with planar to curvilinear contacts appears to have taken place in a consolidated host capable of sustaining brittle fracture, and angular clasts of wehrlite attest to brittle disaggregation of pre-existing cumulates (Fig. 10c,d,g). Overall, the chaotically intermingled units are interpreted to represent zones of episodic mingling and intrusion involving variably crystallized and/or consolidated cumulates in differing thermal/rheological states.

Chromitite

The textural features displayed by chromitites in the Polaris intrusion are analogous to those described above for Tulameen. Chromitite at Polaris occurs in dunite, and less commonly in olivine wehrlite and wehrlite, as centimetre- to metre-scale schlieren of massive chromite and as disrupted blocks of variably deformed chromitite interlayered with dunite (Fig. 11). Layered samples show strong evidence of ductile deformation such as folding (Fig. 11a), and obliteration and/or coalescence of fine layering and reworking of chromite seams into more massive, irregular pods (Fig. 11c). Some outcrops exhibit a jumbled concentration of clasts comprising plastically deformed chromitite layering, massive schlieren, and subrounded fragments of layered chromitite-dunite that show no evidence of ductile deformation (Fig. 11d). These features are consistent with both ductile breakup/reworking and brittle fragmentation of pre-existing chromitite-dunite cumulates followed by transport and redeposition in their current dunite host. In some cases, early ductile deformation/disaggregation and redeposition of layered chromitite-dunite fragments are succeeded by injection

Figure 10 opposite page. Photographs showing contact relationships and textural features exhibited by ultramafic-mafic rocks of the Polaris intrusion. **a)** Metre-scale gradational contacts of olivine clinopyroxenite, olivine wehrlite to wehrlite, and dunite. **b)** Intermingled dunite and olivine clinopyroxenite. The contacts between the ultramafic rocks are sharp and irregular. **c)** Dykes of foliated dunite cutting massive olivine clinopyroxenite. **d)** Complex relationships among dunite, olivine wehrlite, wehrlite, and locally pegmatitic olivine clinopyroxenite. An offset dunite dyke is delineated by a fine-dashed line. **e)** Coarse-grained olivine clinopyroxenite blocks in wehrlite, cut by/intermingled with fine-grained dunite. **f)** Subrounded fragments (<30 cm) of fine- to medium-grained dunite and olivine wehrlite with diffuse boundaries set in a medium-grained wehrlite to olivine-clinopyroxenite matrix. **g)** Angular to subangular tabular xenoliths of wehrlite showing a distinct (flow?) foliation in a coarse-grained phlogopite-hornblende clinopyroxenite. **h)** Heterogeneous fine(fn)- to coarse(crs)-grained hornblende diorite, locally foliated. Hammer for scale in photographs (a–c) is 37 cm in length; pencil magnet in photographs (f–h) is 13 cm in length. Diffuse contacts are shown using a dot-dash line and sharp contacts with a solid line. Abbreviations: Du = dunite, HD = hornblende diorite, OPx = olivine clinopyroxenite, OWe = olivine wehrlite, Peg-OPx = pegmatitic olivine clinopyroxenite, phl-hbl-Cpxt = phlogopite-hornblende clinopyroxenite, We = wehrlite.

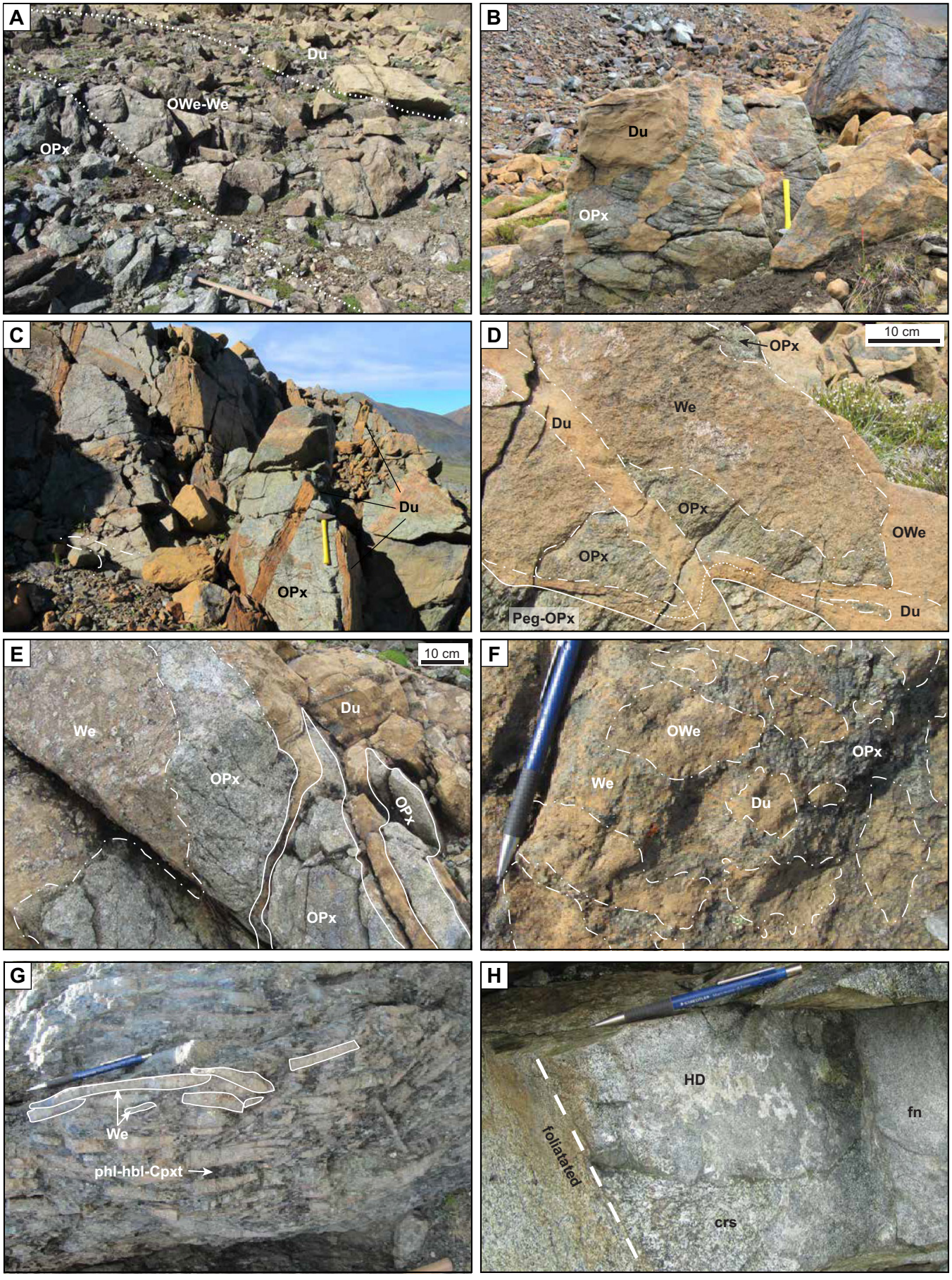
A
Du
OWe-We
OPx
B
Du
OPx
C
Du
OPx
D
10 cm
OPx
We
Du
OPx
OWe
OPx
Peg-OPx
Du
E
10 cm
Du
We
OPx
OPx
OPx
F
OWe
OPx
We
Du
G
We
phl-hbl-Cpxt
H
HD
fn
foliated
crs

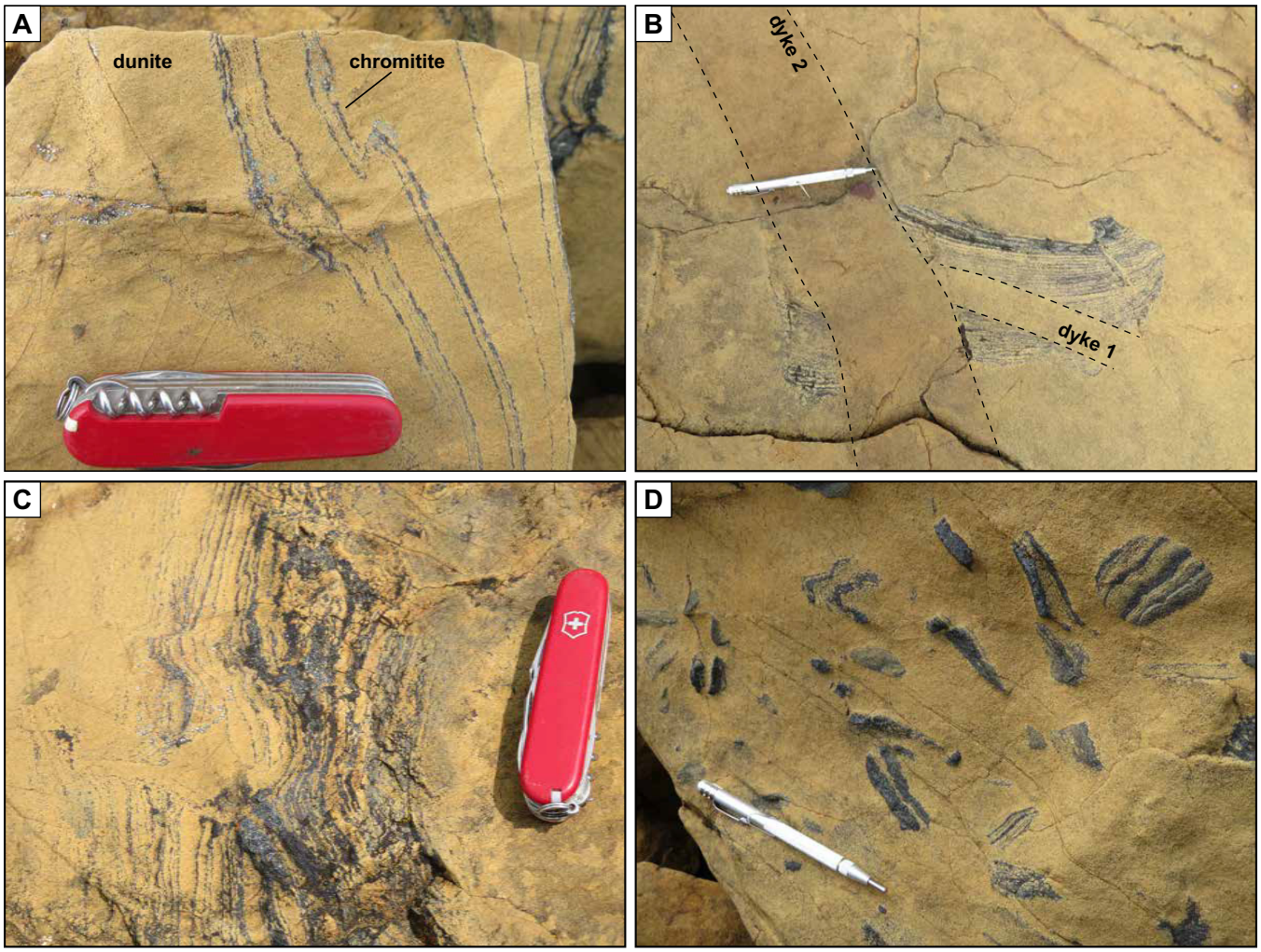

Figure 11. Photographs showing remobilized chromitite in the Polaris intrusion. **a)** Ductile deformation of adcumulate dunite containing thin laminae of chromitite and showing an isolated fold. **b)** Fragment of layered chromitite cut by two generations of dunite (1) and wehrlite (2) dykes, illustrating early ductile deformation/fragmentation of chromitite-dunite followed by late injection of dunite and wehrlite into a consolidated brittle host. **c)** Plastically deformed fragment of well layered chromitite in dunite showing reworking of thin, malleable chromitite layers into more massive, irregular pods of chromitite. **d)** Concentration of fragments comprising plastically deformed chromitite layering, massive schlieren, and subrounded fragments of layered chromitite-dunite showing no evidence of ductile deformation. The variety of textural features is compatible with both ductile breakup/reworking and brittle fragmentation of pre-existing chromitite-dunite cumulates followed by transport and redeposition in their current dunite host. Knife in photographs (a) and (c) is 10 cm in length; pencil magnet in photographs (b) and (d) is 13 cm in length.

of dunite dykes into a consolidated brittle host (Fig. 11b), features similar to those found in the chaotically intermingled units (Fig. 10d). Brittle fragmentation, or possibly early dyke emplacement in coherent layered chromitite-dunite sequences, may account for sharply truncated chromitite schlieren and angular to subangular, centimetre-sized chromitite fragments.

Ni-Cu-PGE Sulphides

Magmatic Ni-Cu(-PGE) sulphides in the Polaris intrusion generally occur in the more evolved ultramafic and mafic rocks in the northwestern and central parts of the intrusion (Fig. 9). The sulphides are hosted by wehrlite, olivine clinopyroxenite, hornblende clinopyroxenite, pegmatitic hornblendite, and gabbro-diorite. The mineralized rocks commonly weather reddish to rusty brown and display prominent malachite staining. The disseminated to locally blebby sulphides comprise mainly pyrrhotite and chalcopyrite with minor pentlandite, pyrite and rare bornite, and may constitute up to 15–20 vol.% of mineralized samples. The composition and textures of the sulphides are demonstrably magmatic as evidenced by ovoid inclusions of formerly immiscible sulphide melt in clinopyroxene and hornblende primocrysts, and irregular films and pockets of interstitial sulphides trapped within the cumulus silicate framework (Fig. 12a–c). Bornite, where present, is magmatic and occurs with chalcopyrite as composite interstitial grains and inclusions in magnetite with negative-crystal outlines. Coexistence of bornite and

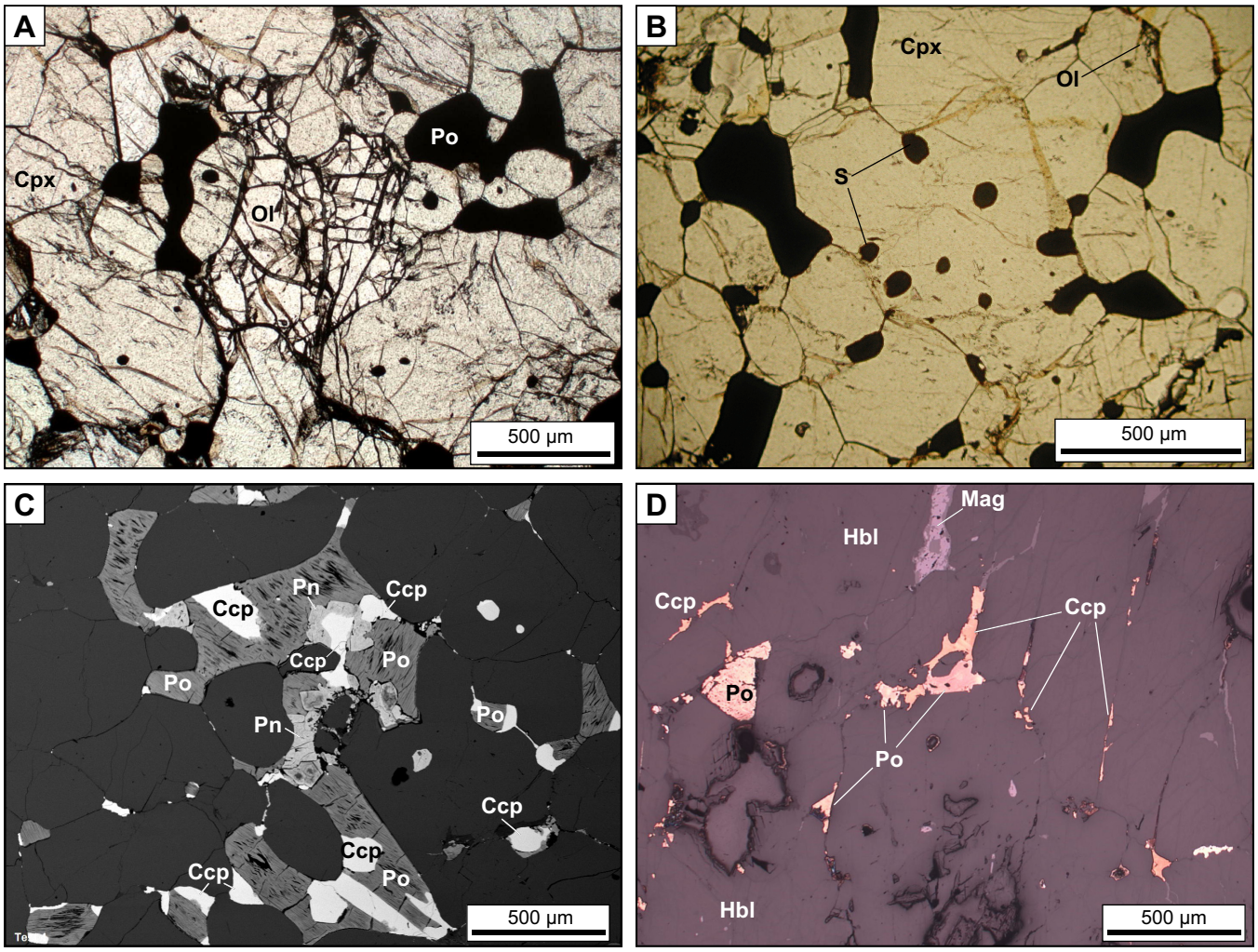

Figure 12. Photographs and images of sulphide-bearing samples from the Polaris intrusion. **a)** Plane-polarized light image of interstitial pyrrhotite in olivine clinopyroxenite. **b)** Plane-polarized light image of disseminated magmatic sulphides in olivine-bearing clinopyroxenite. The rounded shapes of sulphide inclusions in clinopyroxene and along silicate grain boundaries indicate trapping of immiscible sulphide liquid during silicate crystallization and accumulation. **c)** Backscatter electron image of composite interstitial sulphides in olivine clinopyroxenite. **d)** Reflected light image of primary and remobilized fracture-filling sulphides in hornblendite. Scales as noted on each photograph. Abbreviations: Ccp = chalcopyrite, Cpx = clinopyroxene, Hbl = hornblende, Mag = magnetite, Ol = olivine, Pn = pentlandite, Po = pyrrhotite, S = undifferentiated sulphide.

chalcopyrite implies the existence of a Cu-rich sulphide melt, analogous to sulphide assemblages documented above in the Champion zone of the Tulameen intrusion. The copper-rich sulphides commonly display thin alteration rims of covellite. Locally remobilized sulphides occupy thin veinlets or form fine films lining cleavage planes and/or fractures in amphibole (Fig. 12d). The presence of pentlandite and common occurrence of pyrrhotite distinguish Polaris sulphides from the Cu-rich sulphides in the Champion zone. A collection of chalcopyrite-bearing bulk-rock samples from a number of mineralized zones have maximum values of 1.18 wt% Cu, 1.8 g/t Pd and 1.3 g/t Pt (Mowat, 2015), and yield PGE signatures (Pd/Pt = 1.4), similar to those reported herein for Cu-PGE mineralized rocks in the Champion zone. Further work is needed to more completely characterize the mineralogical and geochemical attributes of the mineralization.

REMOBILIZED CUMULATES: VESTIGES OF MAGMA RECHARGE?

The textural features documented above for chromitites, intermingled ultramafic cumulates, and magmatic avalanche deposits in the Tulameen and Polaris intrusions provide evidence for ductile to brittle disaggregation, reworking, and redeposition of pre-existing cumulates in a dynamic magmatic environment. In this section, we have adapted a magma recharge model to explain the commonality of features exhibited by the remobilized cumulates. The model may have general applicability because, for example, chromitites with similar characteristics have been described in many Alaskan-type intrusions (e.g. Nixon et al., 1997; Garuti et al., 2003; Scheel et al., 2009; Anikina et al., 2014).

The mechanical and temporal evolution of an open-system magma-recharge event have been simulated

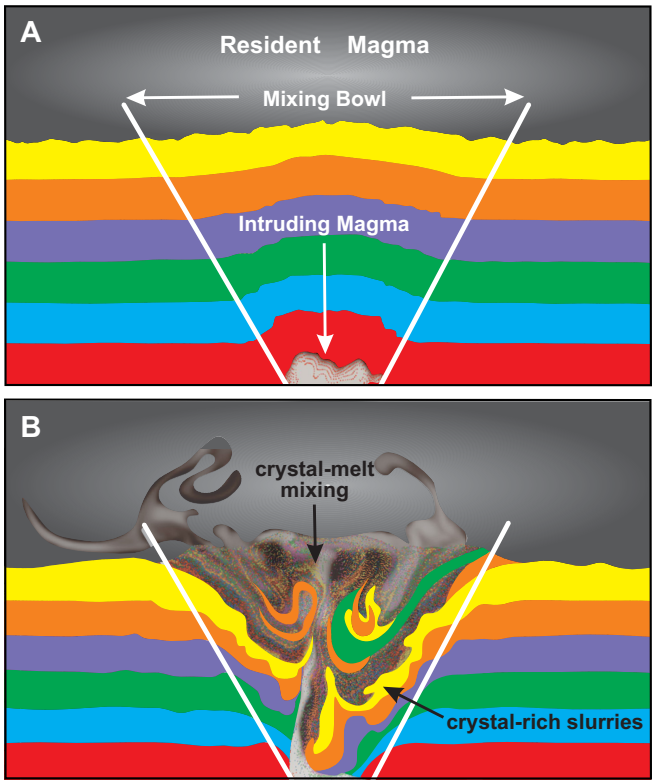

Figure 13. Schematic diagram depicting two stages in the computer simulation of an open-system recharge event (*redrawn from* Schleicher and Bergantz, 2017). **a)** Basaltic magma intrudes an olivine crystal mush with 40% interstitial melt. Crystal cumulates in the mush zone are multi-coloured for tracking purposes; an intruding basaltic melt is shown in mixed grey tones. The intruding magma induces a viscoplastic response in the cumulate pile that creates a mixing bowl. **b)** Hydrogranular dynamics subsequently create a fluidized, well mixed region of crystals and melt in the central part of the mixing bowl. The inferred environments of remobilized ultramafic cumulates in the Tulameen and Polaris Alaskan-type intrusions are discussed in the text within the framework of this model. For a full appreciation of the open-system dynamics, the reader is encouraged to view the video in the online Supplementary Data of Schleicher and Bergantz (2017).

using a computer algorithm to account for the complex interactions of the granular and fluid dynamics of basaltic liquid intruding a partially consolidated olivine-rich cumulate mush (Bergantz et al., 2015; Schleicher et al., 2016; Schleicher and Bergantz, 2017; Fig. 13). Basaltic liquid is injected into the base of crystal mush (crystal:melt ratio = 60:40) as a dyke under isothermal conditions at a constant momentum flux at a sufficiently high rate to overcome the resistance of the mush zone, which behaves as a viscoplastic material (Fig. 13a). The addition of basaltic liquid to the system is accommodated by internal inflation (ballooning) of the magma reservoir or eruption of the resident magma. The mush responds to the new magma influx by vertical expansion and fluidization along bounding crystal-liquid faults of relatively stable configuration that define a region of the mush unlocked by fluidization: referred to as the "mixing bowl" (Fig. 13a). This initial response is followed by block uplift of the crystal mush within the mixing bowl. The intruding liquid eventually penetrates the mush to form a high-porosity chimney for continued throughput of magma carrying entrained crystals from the base to the top of the cumulate pile where the new liquid mixes with resident magma and deposits its remaining crystal cargo on top of the mush (Fig. 13b). After the initial influx, the system reaches a quasi-steady state as the position of the chimney meanders through the mush zone generating granular vortices that expand the well fluidized region in the centre of the mixing bowl. Expansion of this fluidized region is accompanied by crystal slurries moving down the destabilized sides of the mixing bowl towards the base of the magma chamber (Fig. 13b). Termination of the new magma influx causes the mixing bowl to defluidize and collapse leaving a fossil kinematic and compositional footprint distinct from the surrounding undisturbed crystal mush.

Although the geometry of the Tulameen and Polaris magma chambers is not known, two key elements of this open-system recharge model can potentially explain the diversity of features exhibited by remobilized cumulates in these Alaskan-type intrusions: the upward transport and redistribution of material throughout the fluidized, well mixed core of the mixing bowl, and the counterbalanced downward movement of material along the unstable sidewalls.

Olivine-chromite cumulates in the core of the Tulameen intrusion exhibit textural features definitive of mechanical disruption, ductile reworking, and redeposition during crystallization of the dunite (Fig. 6). Framing the natural system in terms of the recharge model, formation of the dunite core involves recycling of early formed, coherent olivine-chromite cumulates, and mixing of recycled crystals from the mush and newly formed crystals from the intruding and/or hybrid melt, leading to the deposition of olivine-chromite cumulates of mixed age and heritage. Although this process must involve disaggregated fragments of dunite, chromitite and layered chromitite-dunite, as well as potentially separated crystals, only the presence of chromitite preserves overt macroscopic evidence of this heritage. The recycled material may be sourced from the unstable sidewall of the magma chamber and/or derived from compacted cumulates below the mush zone that has been disrupted by new magma influx. Ductile deformation of cumulate inclusions is probably initiated during disaggregation shortly after the initial magma influx, and deformation is sustained on termination of the recharge event as the fluidized core of the mush zone deflates and the recycled olivine(-chromite) crystals and inclusion cargo are redeposited. The relatively small size of chromitite schlieren

and layered chromitite-dunite inclusions observed in the dunite core would appear amenable to upward transport and dispersion by hydrogranular currents, depending on the momentum of new magma influx.

The textural relationships between plastically deformed dunite blocks (up to 15 m across) and host clinopyroxenite are interpreted above as evidence for synmagmatic avalanche deposits that involve the gravitational collapse of hot, malleable pre-existing cumulates. These deposits occur throughout the clinopyroxenite unit peripheral to the dunite core (Fig. 2) and include both coherent dunite and clinopyroxenite cumulates. Clasts of the latter are macroscopically visible where enclosed by dunite blocks, which are key markers of the recycling and deformation processes (Fig. 7).

In the recharge model, an environment conducive to the generation of the avalanche deposits is manifest at the margins of the mixing bowl where crystal-charged slurries move downslope towards the conduit (Fig. 13b). In the natural system, thermal gradients would exist between the hot centre of the mixing bowl and cooler wallrocks. By the time the avalanche deposits were generated, the peripheral zones of the intrusion must have cooled sufficiently via heat conduction through the wallrocks to form hot coherent dunite and clinopyroxenite cumulates. These cumulates were subsequently dislodged from the walls of the magma chamber and disrupted blocks cascaded downslope embroiled in the crystal mush to form the avalanche deposits. Ductile deformation of dunite inclusions likely began during disaggregation and continued during transport and deposition in the deeper, hotter regions near the base of the magma chamber. Such processes operating in the sidewall environment may also account for the features exhibited by chaotically intermingled ultramafic cumulates in the Polaris intrusion where the lack of extensive fragmentation may indicate limited downslope movement of cumulates and/or slumping *en masse*.

IMPLICATIONS FOR EXPLORATION

The Cu-PGE mineralization in the Tulameen ultramafic-mafic intrusion represents a unique deposit type for Alaskan-type intrusions, which are better known for chromite-associated platinum mineralization in dunite and the derivative placer deposits. The mineralization has certain attributes in common with Cu-PGE stratiform or reef-style occurrences in layered intrusions. Given the current historic high for the price of Pd (more than double the price of Pt and one and a half times that of Au as of March, 2020), the Pd-enriched nature of the Cu-sulphide mineralization at Tulameen may well become a significant factor in promoting exploration for this deposit style in Alaskan-type intrusions.

The magma-recharge model described above provides an explanation for the occurrence of Pt-rich and Pt-poor chromitites in close proximity in the dunite core of the Tulameen intrusion. The disaggregation of pre-existing olivine-chromite cumulates by an intruding magma, and their entrainment and redistribution by hydrogranular currents throughout the interior of the mixing bowl, as represented by the dunite core, results in the redeposition of dismembered, variably platiniferous chromitites derived from different parts of the original cumulate sequence. The small size and apparently chaotic distribution of the Pt-rich chromitites in bedrock is not conducive to economic exploitation. Unless laterally continuous, platiniferous chromitite horizons in the dunite can be identified, the associated placer deposits are more amenable targets.

FUTURE RESEARCH

U-Pb zircon geochronological and trace element geochemical studies are continuing for representative samples from the Tulameen intrusion, including those collected from Cu-PGE sulphide mineralization in the Champion zone. Samples collected by James Nott for his M.Sc. research at the University of British Columbia on the Polaris intrusion are currently being processed for U-Pb zircon LA-ICP-MS and CA-ID-TIMS geochronology following established workflows.

ACKNOWLEDGMENTS

Funding for this study was provided by NRCan's Targeted Geoscience Initiative Program (TGI- 5) under the Orthomagmatic Ni-Cu-PGE-Cr Ore Systems Project's 'Convergent margin Ni-Cu-PGE-Cr temporal and magmatic evolution', the British Columbia Geological Survey, and a NSERC Discovery Grant to James Scoates. James Nott's research at Polaris is partially supported by a NSERC Canada Graduate Scholarship. Dylan Spence and Abigail Fraser expedited field preparations and provided support throughout the 2018 and 2019 field seasons at Polaris, respectively. Ursula Mowat is thanked for providing a suite of mineralized samples from her claims on Polaris. We thank Wouter Bleeker for thorough and careful review of the manuscript and Valérie Bécu and Elizabeth Ambrose for technical editing and formatting of the final layout.

REFERENCES

Ames, D.E., Kjarsgaard, I.M., McDonald, A.M., and Good, D.J., 2017. Insights into the extreme PGE enrichment of the W Horizon, Marathon Cu-Pd deposit, Coldwell Alkaline Complex, Canada: Platinum-group mineralogy, compositions and genetic implications; Ore Geology Reviews, v. 90, p. 723–747.

Anikina, E., Malitch, K.N., Pushkarev, E.V., and Shmelev, V.R., 2014. The Nizhny Tagil and Volkovsky massifs of the Uralian Platinum Belt, and related deposits; Field Trip Guidebook, Zavaritsky Institute of Geology and Geochemistry, Russian Academy of Sciences, 12th International Platinum Symposium, Yekaterinburg, 48 p.

Annen, C., Blundy, J.D., Leuthold, J., and Sparks, R.S.J., 2015. Construction and evolution of igneous bodies: Towards an integrated perspective of crustal magmatism; Lithos, v. 230, p. 206–221.

Bergantz, G.W., Schleicher, J.M., and Burgisser, A., 2015. Open-system dynamics and mixing in magma mushes; Nature Geoscience, v. 8, p. 793–796.

Brenan, J.M. and Andrews, D., 2001. High-temperature stability of laurite and Ru–Os–Ir alloy and their role in PGE fractionation in mafic magmas; The Canadian Mineralogist, v. 39, p. 341–360.

Colpron, M. and Nelson, J.L., 2011. A digital atlas of terranes for the Northern Cordillera; British Columbia Ministry of Energy and Mines, British Columbia Geological Survey, Geofile 2011–11.

DeCelles, P.G., Ducea, M.N., Kapp, P., and Zandt, G., 2009. Cyclicity in Cordilleran orogenic systems; Nature Geoscience, v. 2, p. 251–257.

Engi, M., Lanari, P., and Kohn, M.J., 2017. Significant ages; an introduction to petrochronology; *in* Reviews in Mineralogy and Geochemistry, (ed.) M.J. Kohn, M., Engi, and P. Lanari;, Mineralogical Society of America and Geochemical Society, Washington, DC, p. 1–12.

Ferri, F., 1997. Nina Creek Group and Lay Range Assemblage, north-central British Columbia: remnants of late Paleozoic oceanic and arc terranes; Canadian Journal of Earth Sciences, v. 34, p. 854–874.

Ferry, J.M. and Watson, E.B., 2007. New thermodynamic models and revised calibrations for the Ti-in-zircon and Zr-in-rutile thermometers; Contributions to Mineralogy and Petrology, v. 154, p. 429–437.

Findlay, D.C., 1963. Petrology of the Tulameen ultramafic complex, Yale District, British Columbia; Ph.D. thesis, Queen's University, Kingston, Ontario, 415 p.

Findlay, D.C., 1969. Origin of the Tulameen ultramafic-gabbro complex, southern British Columbia; Canadian Journal of Earth Sciences, v. 6, p. 399–425.

Fortin, M.-A., Riddle, J., Desjardins-Langlais, Y., and Baker, D.R., 2015. The effect of water on the sulfur concentration at sulfide saturation (SCSS) in natural melts; Geochimica et Cosmochimica Acta, v. 160, p. 100–116.

Garuti, G., Pushkarev, E.V., Zaccarini, F., Cabella, R., and Anikina, E., 2003. Chromite composition and platinum-group mineral assemblage in the Uktus Uralian-Alaskan-type complex (Central Urals, Russia); Mineralium Deposita, v. 38, p. 312–326.

Gehrels, G., Rusmore, M., Woodsworth, G., Crawford, M., Andronicos, C., Hollister, L., Patchett, J., Ducea, M., Butler, R., Klepeis, K., Davidson, C., Friedman, R.M., Haggart, J.W., Mahoney, J.B., Crawford, W., Pearson, D., and Girardi, J., 2009. U-Th-Pb geochronology of the Coast Mountains batholith in north-coastal British Columbia: Constraints on age and tectonic evolution; Geological Society of America Bulletin, v. 121, p. 1341–1361.

Godel, B., 2015. Platinum-group element deposits in layered intrusions: Recent advances in the understanding of the ore forming processes; *in* Layered Intrusions, (ed.) B. Charlier, O. Namur, R. Latypov, and C. Tegner; Springer, Netherlands,,p. 379–432.

Godel, B., Rudashevsky, N.S., Nielsen, T.F.D., Barnes, S.J., and Rudashevsky, V.N., 2014. New constraints on the origin of the Skaergaard intrusion Cu–Pd–Au mineralization: Insights from high-resolution X-ray computed tomography; Lithos, v. 190–191, p. 27–36.

Good, D.J., Cabri, L.J., and Ames, D.E., 2017. PGM Facies variations for Cu-PGE deposits in the Coldwell Alkaline Complex, Ontario, Canada; Ore Geology Reviews, v. 90, p. 748–771.

Greig, C.J., Armstrong, R.L., Harakal, J.E., Runkle, D., and van der Heyden, P., 1992. Geochronometry of the Eagle Plutonic Complex and the Coquihalla area, southwestern British Columbia; Canadian Journal of Earth Sciences, v. 29, p. 812–829.

Grimes, C.B., John, B.E., Cheadle, M.J., Mazdab, F.K., Wooden, J.L., Swapp, S., and Schwartz, J.J., 2009. On the occurrence, trace element geochemistry, and crystallization history of zircon from in situ ocean lithosphere; Contributions to Mineralogy and Petrology, v. 158, p. 757–783.

Haughton, D.R., Roeder, P.L., and Skinner, B.J., 1974. Solubility of sulfur in mafic magmas; Economic Geology, v. 69, p. 451–467.

Himmelberg, G.R. and Loney, R.A., 1995. Characteristics and petrogenesis of Alaskan-type ultramafic-mafic intrusions, southeastern Alaska; United States Geological Survey, Professional Paper 1564, 47 p.

Holwell, D.A. and Keays, R.R., 2014. The formation of low-volume, high-tenor magmatic PGE-Au sulfide mineralization in closed systems: evidence from precious and base metal geochemistry of the Platinova Reef, Skaergaard intrusion, East Greenland; Economic Geology, v. 109, p. 387–406.

Holwell, D.A., Keays, R.R., McDonald, I., and Williams, M.R., 2015. Extreme enrichment of Se, Te, PGE and Au in Cu sulfide microdroplets: evidence from LA-ICP-MS analysis of sulfides in the Skaergaard intrusion, East Greenland; Contributions to Mineralogy and Petrology, v. 170, p. 53.

Irvine, T.N., 1974. Petrology of the Duke Island ultramafic complex, southeastern Alaska; Geological Society of America, Memoir 138, 240 p.

Jackson-Brown, S., 2017. Origin of the Cu-PGE-rich sulphide mineralization in the DJ/DB zone of the Turnagain Alaskan-type intrusion, British Columbia; M.Sc. thesis, University of British Columbia, Vancouver, British Columbia, 290 p.

Jenner, F.E., O'Neill, H.S.C., Arculus, R.J., and Mavrogenes, J.A., 2010. The magnetite crisis in the evolution of arc-related magmas and the initial concentration of Au, Ag and Cu; Journal of Petrology, v. 51, p. 2445–2464.

Johan, Z., 2002. Alaskan-type complexes and their platinum-group-element mineralization; *in* The Geology, Geochemistry, Mineralogy and Mineral Beneficiation of Platinum-group Elements, (ed.) L.J. Cabri; Canadian Institute of Mining, Metallurgy and Petroleum, Special Volume 54, p. 669–719.

Jugo, P.J., Wilke, M., and Botcharnikov, R.E., 2010. Sulfur K-edge XANES analysis of natural and synthetic basaltic glasses: Implications for S speciation and S content as function of oxygen fugacity; Geochimica et Cosmochimica Acta, v. 74, p. 5926–5938.

Keays, R.R. and Tegner, C., 2015. Magma chamber processes in the formation of the low-sulphide magmatic Au–PGE mineralization of the Platinova Reef in the Skaergaard intrusion, East Greenland; Journal of Petrology, v. 56, p. 2319–2340.

Li, C., Ripley, E.M., Oberthür, T., Miller, J.D., and Joslin, G.D., 2008. Textural, mineralogical and stable isotope studies of hydrothermal alteration in the main sulfide zone of the Great Dyke, Zimbabwe and the precious metals zone of the Sonju Lake Intrusion, Minnesota, USA; Mineralium Deposita, v. 43, p. 97–110.

Li, C., Zhang, Z., Li, W., Wang, Y., Sun, T., and Ripley, E.M., 2015. Geochronology, petrology and Hf–S isotope geochemistry of the newly-discovered Xiarihamu magmatic Ni–Cu sulfide

deposit in the Qinghai–Tibet plateau, western China; Lithos, v. 216–217, p. 224–240.

Logan, J.M. and Mihalynuk, M.G., 2014. Tectonic controls on early Mesozoic paired alkaline porphyry deposit belts (Cu-Au±Ag-Pt-Pd-Mo) within the Canadian Cordillera; Economic Geology, v. 109, p. 827–858.

Maier, W.D., 2005. Platinum-group element (PGE) deposits and occurrences: Mineralization styles, genetic concepts, and exploration criteria; Journal of African Earth Sciences, v. 41, p. 165–191.

Maier, W.D., Barnes, S.-J., Gartz, V., and Andrews, G., 2003. Pt-Pd reefs in magnetitites of the Stella layered intrusion, South Africa: A world of new exploration opportunities for platinum group elements; Geology, v. 31, p. 885–888.

Manor, M.J., Scoates, J.S., Nixon, G.T., and Ames, D.E., 2016. The Giant Mascot Ni-Cu-PGE deposit, British Columbia: mineralized conduits in a convergent margin tectonic setting; Economic Geology, v. 111, p. 57–87.

Manor, M.J., Scoates, J.S., Wall, C.J., Nixon, G.T., Friedman, R.M., Amini, M., and Ames, D.E., 2017. Age of the Late Cretaceous ultramafic-hosted Giant Mascot Ni-Cu-PGE deposit, southern Canadian Cordillera: integrating CA-ID-TIMS and LA-ICP-MS U-Pb geochronology and trace element geochemistry of zircon; Economic Geology, v. 112, p. 1395–1418.

Mattinson, J.M., 2005. Zircon U–Pb chemical abrasion ("CA-TIMS") method: Combined annealing and multi-step partial dissolution analysis for improved precision and accuracy of zircon ages; Chemical Geology, v. 220, p. 47–66.

Matzel, J.E., Bowring, S.A., and Miller, R.B., 2006. Time scales of pluton construction at differing crustal levels: Examples from the Mount Stuart and Tenpeak intrusions, North Cascades, Washington; Geological Society of America Bulletin, v. 118, p. 1412–1430.

McDonough, W.F. and Sun, S.-S., 1995. The composition of the Earth; Chemical Geology, v. 120, p. 223–253.

Miller, J.D., Jr., 1999. Geochemical evaluation of platinum group element (PGE) mineralization in the Sonju Lake intrusion, Finland, Minnesota; Minnesota Geological Survey, Information Circular 44, 32 p.

Miller, J.D., Jr., and Ripley, E.M., 1996. Layered intrusions of the Duluth Complex, Minnesota, USA; *in* Layered Intrusions, Developments in Petrology, (ed.) R.G. Cawthorn; Elsevier, v. 15, p. 257–301.

Miller, J.S., Matzel, J.E.P., Miller, C.F., Burgess, S.D., and Miller, R.B., 2007. Zircon growth and recycling during the assembly of large, composite arc plutons; Journal of Volcanology and Geothermal Research, v. 167, p. 282–299.

Monger, J.W.H. and Gibson, H.D., 2019. Mesozoic-Cenozoic deformation in the Canadian Cordillera: The record of a "Continental Bulldozer"?; Tectonophysics, v. 757, p. 153–169.

Mowat, U., 2015. Sampling on the Star 1, 3, 8, 10, 11 and 12 claims; British Columbia Geological Survey, Assessment Report 35680, 88 p.

Mudd, G.M. and Jowitt, S.M., 2014. A detailed assessment of global nickel resource trends and endowments; Economic Geology, v. 109, p. 1813–1841.

Naldrett, A.J., 2004. Magmatic Sulfide Deposits: Geology, Geochemistry and Exploration; Springer-Verlag, Germany, 727 p.

Naldrett, A.J., 2010. Secular variation of magmatic sulfide deposits and their source magmas; Economic Geology, v. 105, p. 669–688.

Nelson, J.L., Colpron, M., and Israel, S., 2013. The Cordillera of British Columbia, Yukon, and Alaska: Tectonics and metallogeny; *in* Tectonics, Metallogeny, and Discovery: The North American Cordillera and Similar Accretionary Settings, (ed.) M. Colpron,T. Bissig, B.J. Rusk, and J.F.M. Thompson; Society of Economic Geologists, Special Paper 17, p. 53–109.

Nixon, G.T., 1998. Ni-Cu sulfide mineralization in the Turnagain Alaskan-type complex; a unique magmatic environment; *in* Geological Fieldwork 1997; Ministry of Employment and Investment, British Columbia Geological Survey, Paper 1998-1, p. 18.1–18.11.

Nixon, G.T., 2018. Geology of the Tulameen Alaskan-type ultramafic-mafic intrusion, British Columbia; British Columbia Ministry of Energy, Mines and Petroleum Resources, British Columbia Geological Survey, Open File 2018-2, scale 1: 20 000.

Nixon, G.T. and Rublee, V.J., 1988. Alaskan-type ultramafic rocks in British Columbia: new concepts of the structure of the Tulameen complex; *in* Geological Fieldwork 1987; British Columbia Ministry of Energy, Mines and Petroleum Resources, British Columbia Geological Survey, Paper 1988-1, p. 281–294.

Nixon, G.T., Cabri, L.J., and Laflamme, J.H.G., 1990. Platinum-group-element mineralization in lode and placer deposits associated with the Tulameen Alaskan-type complex, British Columbia; The Canadian Mineralogist, v. 28, p. 503–535.

Nixon, G.T., Hammack, J.L., Ash, C.H., Cabri, L.J., Case, G., Connelly, J.N., Heaman, L.M., Laflamme, J.H.G., Nuttall, C., Paterson, W.P.E., and Wong, R.H., 1997. Geology and platinum group element mineralization of Alaskan-type ultramafic-mafic complexes in British Columbia; British Columbia Ministry of Employment and Investment, British Columbia Geological Survey, Bulletin 93, 142 p.

Nixon, G.T., Manor, M.J., Jackson-Brown, S., Scoates, J.S., and Ames, D.E., 2015. Magmatic Ni-Cu-PGE sulphide deposits at convergent margins; *in* Targeted Geoscience Initiative 4: Canadian Nickel-Copper-Platinum Group Elements-Chromium Ore Systems - Fertility, Pathfinders, New and Revised Models, (ed.) D.E. Ames and M.G. Houlé, Geological Survey of Canada, Open File 7856, p. 17–34.

Nixon, G.T., Milidragovic, D., and Scoates, J.S., 2019. Convergent margin Ni-Cu-PGE-Cr ore systems: temporal and magmatic evolution; *in* Targeted Geoscience Initiative 5, Grant Program Interim Reports 2018-2019; Geological Survey of Canada, Open File 8620, p. 49–61.

Nixon, G.T., Scheel, J.E., Scoates, J.S., Friedman, R.M., Wall, C.J., Gabites, J., and Jackson-Brown, S., 2020. Syn-accretionary multistage assembly of an Early Jurassic Alaskan-type intrusion in the Canadian Cordillera: U-Pb and $^{40}Ar/^{39}Ar$ geochronology of the Turnagain ultramafic-mafic intrusive complex, Yukon-Tanana terrane; Canadian Journal of Earth Sciences, v. 57, p. 575–600.

Nott, J., Milidragovic, D., Nixon, G.T., and Scoates, J.S., 2020. New geological investigations of the Early Jurassic Polaris ultramafic-mafic Alaskan-type intrusion, north-central British Columbia; *in* Geological Fieldwork 2019; British Columbia Ministry of Energy, Mines, and Petroleum Resources, British Columbia Geological Survey, Paper 2020-01, p. 59–76.

Paterson, S.R. and Ducea, M.N., 2015. Arc magmatic tempos; gathering the evidence; Elements, v. 11, p. 91–98.

Piña, R., 2019. The Ni-Cu-(PGE) Aguablanca Ore Deposit (SW Spain); SpringerBriefs in World Mineral Deposits, Springer International Publishing, Switzerland, 78 p.

Pinsent, R.H., 2002. Ni-Cu-PGE potential of the Giant Mascot and Cogburn ultramafic-mafic bodies, Harrison-Hope area, southwestern British Columbia (092H); *in* Geological Fieldwork 2001; British Columbia Ministry of Energy, Mines and Petroleum Resources, British Columbia Geological Survey, Paper 2002-01, p. 211–236.

Prendergast, M.D., 2000. Layering and precious metals mineralization in the Rincón del Tigre Complex, eastern Bolivia; Economic Geology, v. 95, p. 113–130.

Prichard, H.M., Mondal, S.K., Mukherjee, R., Fisher, P.C., and Giles, N., 2018. Geochemistry and mineralogy of Pd in the magnetitite layer within the upper gabbro of the Mesoarchean Nuasahi Massif (Orissa, India); Mineralium Deposita, v. 53, p. 547–564.

Rublee, V.J., 1989. The structural control of the Tulameen Complex and outlying ultramafic bodies, 92H/7, 10; *in* Exploration in British Columbia 1988; British Columbia Ministry of Energy, Mines and Petroleum Resources, British Columbia Geological Survey,, p. B71–B81.

Rublee, V.J., 1994. Chemical petrology, mineralogy and structure of the Tulameen Complex, Princeton area, British Columbia; M.Sc. thesis, University of Ottawa, Ottawa, Ontario, 183 p.

Samperton, K.M., Schoene, B., Cottle, J.M., Brenhin Keller, C., Crowley, J.L., and Schmitz, M.D., 2015. Magma emplacement, differentiation and cooling in the middle crust: Integrated zircon geochronological-geochemical constraints from the Bergell Intrusion, Central Alps; Chemical Geology, v. 417, p. 322–340.

Scheel, J.E., 2007. Age and origin of the Turnagain Alaskan-type intrusion and associated Ni-sulphide mineralization, north-central British Columbia, Canada; M.Sc. thesis, University of British Columbia, Vancouver, British Columbia, 210 p.

Scheel, J.E., Scoates, J.S., and Nixon, G.T., 2009. Chromian spinel in the Turnagain Alaskan-type ultramafic intrusion, northern British Columbia, Canada; The Canadian Mineralogist, v. 47, p. 63–80.

Schleicher, J.M. and Bergantz, G.W., 2017. The mechanics and temporal evolution of an open-system magmatic intrusion into a crystal-rich magma; Journal of Petrology, v. 58, p. 1059–1072.

Schleicher, J.M., Bergantz, G.W., Breidenthal, R.E., and Burgisser, A., 2016. Time scales of crystal mixing in magma mushes: Crystal mixing; Geophysical Research Letters, v. 43, p. 1543–1550.

Schoene, B., Schaltegger, U., Brack, P., Latkoczy, C., Stracke, A., and Guenther, D., 2012. Rates of magma differentiation and emplacement in a ballooning pluton recorded by U-Pb TIMS-TEA, Adamello Batholith, Italy; Earth and Planetary Science Letters, v. 355–356, p. 162–173.

Scoates, J.S. and Wall, C.J., 2015. Geochronology of Layered Intrusions; *in* Layered Intrusions, (ed.) B. Charlier, O. Namur, R. Latypov, and C. Tegner; Springer, Netherlands, p. 3–74.

Scoates, J.S., Scoates, R.F.J., Wall, C.J., Friedman, R.M., and Couëslan, C.G., 2017. Direct dating of ultramafic sills and mafic intrusions associated with Ni-sulfide mineralization in the Thompson Nickel Belt, Manitoba, Canada; Economic Geology, v. 112, p. 675–692.

Song, X.-Y., Yi, J.-N., Chen, L.-M., She, Y.-W., Liu, C.-Z., Dang, X.-Y., Yang, Q.-A., and Wu, S.-K., 2016. The giant Xiarihamu Ni-Co Sulfide deposit in the East Kunlun Orogenic Belt, northern Tibet Plateau, China; Economic Geology, v. 111, p. 29–55.

Ver Hoeve, T.J., Scoates, J.S., Wall, C.J., Weis, D., and Amini, M., 2018. A temperature-composition framework for crystallization of fractionated interstitial melt in the Bushveld Complex from trace element systematics of zircon and rutile; Journal of Petrology, v. 59, p. 1383–1416.

Wall, C.J., Scoates, J.S., Weis, D., Friedman, R.M., Amini, M., and Meurer, W.P., 2018. The Stillwater Complex: integrating zircon geochronological and geochemical constraints on the age, emplacement history and crystallization of a large, open-system layered intrusion; Journal of Petrology, v. 59, p. 153–190.

Weiser, T.W., 2002. Platinum-group minerals (PGM) in placer deposits; *in* The Geology, Geochemistry, Mineralogy and Mineral Beneficiation of Platinum-group Elements, (ed.) L.J. Cabri; Canadian Institute of Mining, Metallurgy and Petroleum, Special Volume 54, p. 721–756.

Wohlgemuth-Ueberwasser, C.C., Fonseca, R.O.C., Ballhaus, C., and Berndt, J., 2013. Sulfide oxidation as a process for the formation of copper-rich magmatic sulfides; Mineralium Deposita, v. 48, p. 115–127.

Appendix
Publications related to the TGI-5 Ni-Cu-PGE-Cr Project (2015–2020) and legacies of the TGI-4 Ni-Cu-PGE-Cr Project (2010–2015)

PEER-REVIEWED JOURNAL PUBLICATIONS

Ames, D.E., Kjarsgaard, I.M., McDonald, A.M., and Good, D.J., 2017. Insights into the extreme PGE enrichment of the W Horizon, Marathon Cu-Pd deposit, Coldwell Alkaline Complex, Canada: platinum-group mineralogy, compositions and genetic implications; Ore Geology Reviews, v. 90, p. 723–747.

Brzozowski, M.J., Samson, I.M., Gagnon, J.E., Linnen, R.L., Good, D.J., Ames, D.E., and Flemming, R., 2018. Controls on the chemistry of minerals in late-stage veins and implications for exploration vectoring tools for mineral deposits: An example from the Marathon Cu-Pd deposit, Ontario, Canada; Journal of Geochemical Exploration, v. 190, p. 109–129.

Davey S.C., Bleeker, W., Kamo, S.L., Vuollo, J., Ernst, R.E., and Cousens, B.L., 2020. Archean block rotation in Western Karelia: Resolving dyke swarm patterns in metacraton Karelia-Kola for a refined paleogeographic reconstruction of supercraton Superia; Lithos, v. 368–369, p. 1–24.

Davey, S.C., Bleeker, W., Kamo, S.L., Ernst, R.E., Cousens, B., Chamberlain, K., Vuollo, J., and Huhma, H., submitted. Evidence for a single large igneous province at 2.11 Ga across supercraton Superia; Journal of Petrology.

Kastek, N., Ernst, R.E., Cousens, B.L., Kamo, S.L., Bleeker, W., Söderlund, U., Baragar, W.R.A., and Sylvester, P., 2018. U-Pb Geochronology and geochemistry of the Povungnituk Group of the Cape Smith Belt: Part of a craton-scale circa 2.0 Ga Minto-Povungnituk large igneous province, northern Superior craton; Lithos, v. 320, p. 315–331.

Hiebert, R.S., Bekker, A., Houlé, M.G., and Rouxel, O.J., 2018. Depositional setting of the late Archean Fe oxide- and sulfide-bearing chert and graphitic argillite in the Shaw Dome, Abitibi greenstone belt, Canada; Precambrian Research, v. 311, p. 98–116.

Hiebert, R.S., Bekker, A., Houlé, M.G., Wing, B.A., and Rouxel, O.J., 2016. Tracing sources of crustal contamination using multiple S and Fe isotopes in the Hart komatiite-associated Ni–Cu–PGE sulfide deposit, Abitibi greenstone belt, Ontario, Canada; Mineralium Deposita, v. 51, p. 919–935. https://doi.org/10.1007/s00126-016-0644-1

Houlé, M.G., Lesher, C.M., and Préfontaine, S., 2017. Physical Volcanology of Komatiites and Ni-Cu-(PGE) Deposits of the southern Abitibi Greenstone Belt; *in* Abitibi Base and Precious Metal Deposits, southern Abitibi Greenstone Belt, Canada, (ed.) T. Monecke, P. Mercier-Langevin, and B. Dubé; Reviews in Economic Geology, v. 19, p. 103–132.

Huang, X.-W., Sappin, A.-A., Boutroy, É., Beaudoin, G., and Makvandi, S., 2019. Trace element composition of igneous and hydrothermal magnetite from porphyry deposits: Relationship to deposit subtypes and magmatic affinity; Economic Geology, v. 114, p. 917–952.

Lesher, C.M., Carson, H.J.E., and Houlé, M.G., 2019. Genesis of chromite deposits by dynamic upgrading of Fe±Ti oxide xenocrysts; Geology, v. 47, p. 207–210 https://doi.org/10.1130/G45448.1

Manor, M.J., Scoates, J.S., Nixon, G.T., and Ames, D.E., 2016. The Giant Mascot Ni-Cu-PGE deposit, British Columbia: mineralized conduits in a convergent margin tectonic setting; Economic Geology, v. 111, p. 57–87.

Manor, M.J., Scoates, J.S., Wall, C.J., Nixon, G.T., Friedman, R.M., Amini, M., and Ames, D.E., 2017. Age of the Late Cretaceous ultramafic-hosted Giant Mascot Ni-Cu-PGE deposit, southern Canadian Cordillera: integrating CA-ID-TIMS and LA-ICP-MS U-Pb geochronology and trace element geochemistry of zircon; Economic Geology, v. 112, p. 1395–1418.

McClenaghan, M.B., Plouffe, A., Paulen, R.C., Houlé, M.G., Jackson, S.E., and Peter, J.M., 2016. Overview of Indicator Mineral Research at the Geological Survey of Canada - An Update; EXPLORE, Newsletter for the Association of Applied Geochemists, v. 170, p. 1–15.

Motomura, K., Kiyokawa, S., Ikehara, M., Sano, T., Bleeker, W., Tanaka, K., Miki, T., and Sano, Y., submitted. A redox fluctuation and δ^{13}Corg and δ^{34}S perturbations recorded in the 1.9 Ga Nuvilik Formation of the Cape Smith belt, Canada; Earth and Planetary Science Letters.

Sappin, A.-A., Houlé, M.G., Lesher, C.M., McNicoll, V., Vaillancourt, C., and Kamber, B.S., 2016. Age constraints and geochemical evolution of the Neoarchean mafic-ultramafic Wabassi Intrusive Complex in the Miminiska-Fort Hope greenstone belt, Superior Province, Canada; Precambrian Research, v. 286, p. 101–125.

Sappin, A.-A., Guilmette, C., Goutier, J., and Beaudoin, G., 2018. Geochemistry of Mesoarchean felsic to ultramafic

Appendix: Publications related to the TGI-5 Ni-Cu-PGE-Cr Project (2015–2020) and legacies of the TGI-4 Ni-Cu-PGE-Cr Project (2010–2015); *in* Targeted Geoscience Initiative 5: Advances in the understanding of Canadian Ni-Cu-PGE and Cr ore systems – Examples from the Midcontinent Rift, the Circum-Superior Belt, the Archean Superior Province, and Cordilleran Alaskan-type intrusions, (ed.) W. Bleeker and M.G. Houlé; Geological Survey of Canada, Open File 8722, p. 219–225.

volcanic rocks of the Lac Guyer area, La Grande Subprovince (Canada): Evidence for plume-related magmatism in a rift setting; Precambrian Research, v. 316, p. 83–102.

Shahabi Far, M., Samson, I.M., Gagnon, J.E., Good, D.J., Linnen, R.L., Layne, G.D., and Wing, B.A., 2018. Identifying externally derived sulfur in conduit-type Cu-platinum-group element deposits; the importance of multiple sulfur isotope studies; Geology, v. 46, p. 235–238.

GOVERNMENT PUBLICATIONS

Adibpour, M., Jugo, P.J., and Ames, D.E., 2015. Trace element distribution in sulphide assemblages of the Levack-Morrison ore system, Sudbury, Ontario: Looking for chemical fingerprints of mineralization processes; *in* Targeted Geoscience Initiative 4: Canadian NickelCopper-Platinum Group Elements-Chromium Ore Systems — Fertility, Pathfinders, New and Revised Models, (ed.) D.E. Ames and M.G. Houlé; Geological Survey of Canada, Open File 7856, p. 257–268.

Ames, D.E. and Houlé, M.G., 2015. A synthesis of the TGI-4 Canadian nickel-copper-platinum group elements-chromium ore systems project — revised and new genetic models and exploration tools for Ni-Cu-PGE, Cr-(PGE), Fe-Ti-V-(P), and PGE-Cu deposits; *in* Targeted Geoscience Initiative 4: Canadian Nickel-Copper-Platinum Group Elements-Chromium Ore Systems — Fertility, Pathfinders, New and Revised Models, (ed.) D.E. Ames and M.G. Houlé; Geological Survey of Canada, Open File 7856, p. 1–15.

Ames, D.E. and Tuba, G., 2015. Epidote-amphibole and accessory phase mineral chemistry as a vector to low-sulphide platinum group element mineralization, Sudbury: laser ablation ICP-MS trace element study of hydrothermal alteration; *in* Targeted Geoscience Initiative 4: Canadian Nickel-Copper-Platinum Group Elements-Chromium Ore Systems — Fertility, Pathfinders, New and Revised Models, (ed.) D.E. Ames and M.G. Houlé; Geological Survey of Canada, Open File 7856, p. 269–286.

Bécu, V. and Houlé, M.G., 2015. Chromite occurrences of the E-Ext stripped outcrop, Mayville intrusion, Bird River greenstone belt, southeastern Manitoba; Geological Survey of Canada, Scientific Presentation 28, 1 sheet, https://doi.org/10.4095/296135

Bécu, V., Houlé, M.G., McNicoll, V.J., Yang, X.M., and Gilbert, H.P., 2015. Mafic intrusive rocks from the Bird River intrusive suite, Bird River greenstone belt, southeast Manitoba; *in* Targeted Geoscience Initiative 4: Canadian Nickel-Copper-Platinum Group Elements Chromium Ore Systems — Fertility, Pathfinders, New and Revised Models, (ed.) D.E. Ames and M.G. Houlé; Geological Survey of Canada, Open File 7856, p. 49–60.

Bécu, V., Houlé, M.G., McNicoll, V.J., Yang, X.M., and Gilbert, H.P., 2015. New insights from textural, petrographic, and geochemical investigation of the gabbroic rocks of the Bird River intrusive event within the Bird River greenstone belt, southeastern Manitoba; Geological Survey of Canada, Scientific Presentation 27, 1 sheet. https://doi.org/10.4095/296133

Bédard, M.-P., Houlé, M.G., Hébert, R., Goutier, J., 2017. Étude pétrographique de l'intrusion ultramafique chromitifère du lac des Montagnes, Baie-James, Québec; Geological Survey of Canada, Scientific Presentation 55, 1 sheet. https://doi.org/10.4095/299839

Bédard, M.-P., Houlé, M.G., and Huot, F., 2018. Caractérisation des filons-couches mafiques et ultramafiques de la Zone de Gerido dans la région des Lacs Qamaniik, Fosse du Labrador, Nunavik, Québec; Geological Survey of Canada, Scientific Presentation 89, 1 sheet.

Bleeker, W., 2020. Preface; *in* Targeted Geoscience Initiative 5: Advances in the understanding of Canadian Ni-Cu-PGE and Cr ore systems – Examples from the Midcontinent Rift, the Circum-Superior Belt, the Archean Superior Province, and Cordilleran Alaskan-type intrusions, (ed.) W. Bleeker and M.G. Houlé; Geological Survey of Canada, Open File 8722, p. 1–6. https://doi.org/10.4095/326835

Bleeker, W. and Ames, D.E., 2017. System-scale and deposit-scale controls on Ni-Cu-PGE mineralization in cratonic areas and their margins; *in* Targeted Geoscience Initiative – 2016 Report of Activities, (ed.) N. Rogers; Geological Survey of Canada, Open File 8199, p. 47-53. https://doi:10.4095/299573

Bleeker, W. and Houlé, M.G. (ed.), 2020. Targeted Geoscience Initiative 5: Advances in the understanding of Canadian Ni-Cu-PGE and Cr ore systems – Examples from the Midcontinent Rift, the Circum-Superior Belt, the Archean Superior Province, and Cordilleran Alaska-type intursions; Geological Survey of Canada, Open File 8722, 225 p. https://doi.org/10.4095/326702

Bleeker, W. and Kamo, S.L., 2018. Extent, origin, and deposit-scale controls of the 1883 Ma Circum-Superior large igneous province, northern Manitoba, Ontario, Quebec, Nunavut and Labrador; *in* Targeted Geoscience Initiative: 2017 report of activities, volume 2, (ed.) N. Rogers; Geological Survey of Canada, Open File 8373, p. 5–14. https://doi.org/10.4095/306592

Bleeker, W. and Kamo, S., 2020. Structural-stratigraphic setting and U-Pb geochronology of Ni-Cu-Co-PGE ore environments in the central Cape Smith Belt, Circum-Superior Belt; *in* Targeted Geoscience Initiative 5: Advances in the understanding of Canadian Ni-Cu-PGE and Cr ore systems – Examples from the Midcontinent Rift, the Circum-Superior Belt, the Archean Superior Province, and Cordilleran Alaskan-type intrusions, (ed.) W. Bleeker and M.G. Houlé; Geological Survey of Canada, Open File 8722, p. 65–98. https://doi.org/10.4095/326882

Bleeker, W., Kamo, S.L., Ames, D.E., and Davis, D., 2015. New field observations and U-Pb ages in the Sudbury

area: toward a detailed cross-section through the deformed Sudbury Structure; *in* Targeted Geoscience Initiative 4: Canadian Nickel-Copper-Platinum Group Elements-Chromium Ore Systems — Fertility, Pathfinders, New and Revised Models, (ed.) D.E. Ames and M.G. Houlé; Geological Survey of Canada, Open File 7856, p. 151–166.

Bleeker, W., Liikane, D.A., Smith, J., Hamilton, M., Kamo, S.L., Cundari, R., Easton, M., and Hollings, P., 2018. Controls on the localization and timing of mineralized intrusions in intra-continental rift systems, with a specific focus on the ca. 1.1 Ga Mid-continent Rift system; *in* Targeted Geoscience Initiative: 2017 report of activities, volume 2, (ed.) N. Rogers; Geological Survey of Canada, Open File 8373, p. 15–27. https://doi.org/10.4095/306594

Bleeker, W., Smith, J., Hamilton, M., Kamo, S., Liikane, D., Hollings, P., Cundari, R., Easton, M., and Davis, D., 2020. The Midcontinent Rift and its mineral systems: Overview and temporal constraints of Ni-Cu-PGE mineralized intrusions; *in* Targeted Geoscience Initiative 5: Advances in the understanding of Canadian Ni-Cu-PGE and Cr ore systems – Examples from the Midcontinent Rift, the Circum-Superior Belt, the Archean Superior Province, and Cordilleran Alaskan-type intrusions, (ed.) W. Bleeker and M.G. Houlé; Geological Survey of Canada, Open File 8722, p. 7–35. https://doi.org/10.4095/326880

Brzozowski, M.J., Samson, I.M., Gagnon, J.E., Linnen, R.L., Good, D.J., Ames, D.E., and Flemming, R.L., 2015. Variation in vein mineralogy and mineral chemistry around the Marathon Cu-Pd deposit, Ontario: Insights into the development of an exploration tool; *in* Targeted Geoscience Initiative 4: Canadian Nickel-Copper-Platinum Group Elements-Chromium Ore Systems — Fertility, Pathfinders, New and Revised Models, (ed.) D.E. Ames and M.G. Houlé; Geological Survey of Canada, Open File 7856, p. 245–255.

Carson, H.J.E., Lesher, C.M., and Houlé, M.G., 2015. Geochemistry and petrogenesis of the Black Thor intrusive complex and associated chromite mineralization, McFaulds Lake greenstone belt, Ontario; *in* Targeted Geoscience Initiative 4: Canadian Nickel-Copper-Platinum Group Elements-Chromium Ore Systems — Fertility, Pathfinders, New and Revised Models, (ed.) D.E. Ames and M.G. Houlé; Geological Survey of Canada, Open File 7856, p. 87–102.

Chung, C.-J., Franklin, J.M., Hillary, E., and Houlé, M.G., in prep. Technical Report on Development of a GIS-based System for Assessment of Discovery Potential Using an Expert-Defined Nickel Deposit Model and Digital Geological Maps Including Nickel potential maps in Shaw Dome and Dundonald areas (Timmins, ON), Melville Peninsula and Committee Bay areas (Nunavut) and Slave Province (Northwest Territories); Geological Survey of Canada, Open File 8661.

Dare, S.A.S., Ames, D.E., Lightfoot, P.C., Barnes, S.-J., and Beaudoin, G., 2015. Trace elements in Fe-oxide minerals from fertile and barren igneous complexes: Investigating their use as a vectoring tool for Ni-Cu-PGE sulphide mineralization; *in* Targeted Geoscience Initiative 4: Canadian Nickel-Copper-Platinum Group Elements-Chromium Ore Systems — Fertility, Pathfinders, New and Revised Models, (ed.) D.E. Ames and M.G. Houlé; Geological Survey of Canada, Open File 7856, p. 175–185.

Davey, S., Bleeker, W., Kamo, S., Davis, D., Easton, M., and Sutcliffe, R.H., 2019. Ni-Cu-PGE potential of the Nipissing sills as part of the ca. 2.2 Ga Ungava large igneous province; *in* Targeted Geoscience Initiative: 2018 report of activities, (ed.) N. Rogers; Geological Survey of Canada, Open File 8549, p. 403–419. https://doi.org/10.4095/313675

Hanley J.J., MacMillan, M.A., Kerr, M.J., Watts, K.M., Warren, M.R., and Ames, D.E., 2015. Recent advances in fluid and melt inclusion and applied mineralogical research in the Sudbury mining camp: improving ore genesis models and exploration success; *in* Targeted Geoscience Initiative 4: Canadian Nickel-Copper-Platinum Group Elements-Chromium Ore Systems — Fertility, Pathfinders, New and Revised Models, (ed.) D.E. Ames and M.G. Houlé; Geological Survey of Canada, Open File 7856, p. 209–231.

Hiebert, R.S., Bekker, A., Houlé, M.G., Rouxel, O.J., and Wing, B.A., 2015. Identifying and tracing crustal contamination in the Hart komatiite-associated Ni-Cu-(PGE) deposit using multiple S and Fe isotopes: Abitibi greenstone belt, Ontario; *in* Targeted Geoscience Initiative 4: Canadian Nickel-Copper-Platinum Group Elements-Chromium Ore Systems — Fertility, Pathfinders, New and Revised Models, (ed.) D.E. Ames and M.G. Houlé; Geological Survey of Canada, Open File 7856, p. 197–207.

Houlé, M.G. and Préfontaine, S, 2017. Geology and mineralization in the Potter Mine area, Munro Township (Day 2 - part 1): Precious- and base-metal deposits of the southern Abitibi greenstone belt, Superior Province, Ontario and Quebec, 14th Biennial Society for Geology Applied to Mineral Deposits meeting field trip guidebook, (ed.) P. Mercier-Langevin, J. Goutier, and B. Dubé; Geological Survey of Canada, Open File 8317, p. 13–28. https://doi.org/10.4095/306254

Houlé, M.G., Goutier, J., Sappin, A.-A., and McNicoll, V.J., 2015. Regional characterization of ultramafic to mafic intrusions in the La Grande Rivière and Eastmain domains, Superior Province, Quebec; *in* Targeted Geoscience Initiative 4: Canadian Nickel-Copper-Platinum Group Elements-Chromium Ore Systems — Fertility, Pathfinders, New and Revised Models, (ed.) D.E. Ames and M.G. Houlé; Geological Survey of Canada, Open File 7856, p. 125–137.

Houlé, M.G., Lesher, C.M., McNicoll, V.J., Metsaranta, R.T., Sappin, A.-A., Goutier, J., Bécu, V., Gilbert, H.P., and Yang, X.M., 2015. Temporal and spatial distribution of magmatic Cr-(PGE), Ni-Cu-(PGE), and Fe-Ti-(V) deposits in the Bird River–Uchi–OxfordStull–La

Grande Rivière–Eastmain domains: a new metallogenic province within the Superior Craton; *in* Targeted Geoscience Initiative 4: Canadian Nickel-Copper-Platinum Group Elements-Chromium Ore Systems — Fertility, Pathfinders, New and Revised Models, (ed.) D.E. Ames and M.G. Houlé; Geological Survey of Cana da, Open File 7856, p. 35–48.

Houlé, M.G., Lesher, C.M., McNicoll, V.J., and Bécu, V., 2017. Ni-Cr Metallotect: Synthesis, updates, and revised models for the Superior Province; *in* Targeted Geoscience Initiative – 2016 Report of Activities, (ed.) N. Rogers; Geological Survey of Canada, Open File 8199, p. 59–61. https://doi:10.4095/299573

Houlé, M.G., Lesher, C.M., Schetselaar, E.M., Metsaranta, R.T., and McNicoll, V.J., 2017. Architecture of magmatic conduits in Cr-(PGE)/Ni-Cu-(PGE) ore systems; *in* Targeted Geoscience Initiative – 2016 Report of Activities, (ed.) N. Rogers; Geological Survey of Canada, Open File 8199, p. 55–58. https://doi:10.4095/ 299573

Houlé, M.G., Lesher, C.M., and Sappin, A.-A., 2019. Overview of chromium, Fe-Ti-V and Ni-Cu-PGE metal endowment of the Superior Province; *in* Targeted Geoscience Initiative: 2018 report of activities, (ed.) N. Rogers; Geological Survey of Canada, Open File 8549, p. 433–440. https://doi.org/10.4095/313677

Houlé, M.G., Lesher, C.M., Metsaranta, R.T., and Sappin, A.-A., 2019. Architecture of magmatic conduits in chromium-PGE and Ni-Cu-PGE ore systems in Superior Province: example from the 'Ring of Fire' region, Ontario; *in* Targeted Geoscience Initiative: 2018 report of activities, (ed.) N. Rogers; Geological Survey of Canada, Open File 8549, p. 441–448. https://doi.org/ 10.4095/313678

Houlé, M.G., Lesher, C.M., Sappin, A.-A., Bédard, M.-P., Goutier, J., and Yang, X.M., 2020a. Overview of Ni-Cu-(PGE), Cr-(PGE), and Fe-Ti-V magmatic mineralization in the Superior Province: Insights on metallotects and metal endowment; *in* Targeted Geoscience Initiative 5: Advances in the understanding of Canadian Ni-Cu-PGE and Cr ore systems – Examples from the Midcontinent Rift, the Circum-Superior Belt, the Archean Superior Province, and Cordilleran Alaskan-type intrusions, (ed.) W. Bleeker and M.G. Houlé; Geological Survey of Canada, Open File 8722, p. 117–139. https://doi.org/ 10.4095/326890

Houlé, M.G., Lesher, C.M., Metsaranta, R.T., Sappin, A.-A., Carson, H.J.E., Schetselaar, E.M., McNicoll, V., and Laudadio, A., 2020b. Magmatic architecture of the Esker intrusive complex in the Ring of Fire intrusive suite, McFaulds Lake greenstone belt, Superior Province, Ontario: Implications for the genesis of Cr and Ni-Cu-(PGE) mineralization in an inflationary dyke-chonolith-sill complex; *in* Targeted Geoscience Initiative 5: Advances in the understanding of Canadian Ni-Cu-PGE and Cr ore systems – Examples from the Midcontinent Rift, the Circum-Superior Belt, the Archean Superior Province, and Cordilleran Alaskan-type intrusions, (ed.) W. Bleeker and M.G. Houlé; Geological Survey of Canada, Open File 8722, p. 141–163. https://doi.org/10.4095/ 326892

Houlé, M.G., Bandyayera, D., Bécu, V., and Bédard, M.-P., in press. Minéralisations chromifères et nickélifères associées à la Suite mafique-ultramafique de Caumont dans le secteur de Nemiscau, Eeyou Istchee Baie-James, Québec, Canada; Geological Survey of Canada; Scientific Presentation.

Kontak, D.J., MacInnis, L.M., Ames, D.E., Rayner, N.M., and Joyce, N., 2015. A geological, petrological, and geochronological study of the Grey Gabbro unit of the Podolsky Cu-(Ni)-PGE deposit, Sudbury, Ontario, with a focus on the alteration related to the formation of sharp-walled chalcopyrite veins; *in* Targeted Geoscience Initiative 4: Canadian Nickel-Copper-Platinum Group Elements-Chromium Ore Systems — Fertility, Pathfinders, New and Revised Models, (ed.) D.E. Ames and M.G. Houlé; Geological Survey of Canada, Open File 7856, p. 287–301.

Kuzmich, B., Hollings, P., and Houlé, M.G., 2015a. Petrogenesis of the ferrogabbroic intrusions and associated Fe-Ti-V-(P) mineralization within the McFaulds greenstone belt, Superior Province, northern Ontario; *in* Targeted Geoscience Initiative 4: Canadian Nickel-Copper-Platinum Group Elements-Chromium Ore Systems — Fertility, Pathfinders, New and Revised Models, (ed.) D.E. Ames and M.G. Houlé; Geological Survey of Canada, Open File 7856, p. 115–123.

Kuzmich, B., Hollings, P., and Houlé, M.G., 2015b. Lithogeochemistry of iron-titanium-vanadium-phosphorus mineralized mafic intrusions in the McFaulds Lake area, northern Ontario; Ontario Geological Survey, Miscellaneous Release—Data 318.

Laudadio, A.B., Schetselaar, E., Houlé, M.G., and Samson, C., 2018a. 3D geological modelling of the Double Eagle – Black Thor intrusive complexes, McFaulds Lake greenstone belt, Ontario; *in* Targeted Geoscience Initiative: 2017 report of activities, volume 2, (ed.) N. Rogers; Geological Survey of Canada, Open File 8373, p. 35–41. https://doi.org/10.4095/306599

Laudadio, A.B, Schetselaar, E., and Houlé, M.G., 2018b. 3D geological modelling of the Double Eagle-Black Thor intrusive complexes, McFaulds Lake Greenstone Belt, Ontario, Canada; Geological Survey of Canada, Scientific Presentation 82, 1 sheet.

Lesher, C.M. and Houlé, M.G., in press. Geology, physical volcanology, and Ni-Cu-(PGE) deposits of the Raglan area, Cape Smith Belt, Nunavik, Québec, Canada; A Field Trip to the 14th Biennial Society for Geology Applied to Mineral Deposits meeting; Geological Survey of Canada, Open File 8350, 110 p.

McKevitt, D.J., Houlé, M.G., and Lesher, C.M., 2018a. Investigation of ultramafic to mafic komatiitic units within the Raglan Block within the Cape Smith Belt, Nunavik, northern Quebec; *in* Targeted Geoscience

Initiative: 2017 report of activities, volume 1, (ed.) N. Rogers; Geological Survey of Canada, Open File 8358, p. 169–172. http://doi.org/10.4095/306470

McKevitt, Lesher, C.M., and Houlé, M.G., 2018b. Geology and geochemistry of mafic-ultramafic sills in the Northern Permits, Raglan Ni-Cu-(PGE) District, Cape Smith Belt, Nunavik, Quebec; Geological Survey of Canada, Scientific Presentation 90, 1 sheet., https://doi.org/10.4095/308353

McKevitt, D.J., Lesher, C.M. and Houlé, M.G., 2019. Volcanology, geochemistry and petrogenesis of the Expo-Raglan magmatic system in the eastern Cape Smith Belt, Nunavik, northern Quebec; *in* Targeted Geoscience Initiative: 2018 report of activities, (ed.) N. Rogers; Geological Survey of Canada, Open File 8549, p. 393–401. https://doi.org/10.4095/313674

McKevitt, D.J., Lesher, C.M., and Houlé, M.G., 2020. Regional lithogeochemical synthesis of mafic-ultramafic volcanic and intrusive rocks in the Cape Smith Belt, Nunavik, northern Quebec; *in* Targeted Geoscience Initiative 5: Advances in the understanding of Canadian Ni-Cu-PGE and Cr ore systems – Examples from the Midcontinent Rift, the Circum-Superior Belt, the Archean Superior Province, and Cordilleran Alaskan-type intrusions, (ed.) W. Bleeker and M.G. Houlé; Geological Survey of Canada, Open File 8722, p. 99–115. https://doi.org/10.4095/326883

Metsaranta, R.T., Houlé, M.G., McNicoll, V.J., and Kamo, S.L., 2015. Revised geological framework for the McFaulds Lake greenstone belt, Ontario; *in* Targeted Geoscience Initiative 4: Canadian Nickel-Copper-Platinum Group Elements-Chromium Ore Systems — Fertility, Pathfinders, New and Revised Models, (ed.) D.E. Ames and M.G. Houlé; Geological Survey of Canada, Open File 7856, p. 61–73.

Metsaranta, R.T. and Houlé, M.G., 2017a. Geochronology, mineral deposit, drill-core relogging and drill-core compilation data from the Winiskisis Channel, McFaulds Lake and Highbank Lake areas, "Ring of Fire" region, northern Ontario; Ontario Geological Survey, Miscellaneous Release—Data 343.

Metsaranta, R.T. and Houlé, M.G., 2017b. Precambrian geology of the Winiskisis Channel area, "Ring of Fire" region, Ontario—Northern sheet; Ontario Geological Survey, Preliminary Map P.3804; Geological Survey of Canada, Open File 8200, scale 1:100 000. http://doi.org/10.4095/ 299708229

Metsaranta, R.T. and Houlé, M.G., 2017c. Precambrian geology of the McFaulds Lake area, "Ring of Fire" region, Ontario—Central sheet; Ontario Geological Survey, Preliminary Map P.3805; Geological Survey of Canada, Open File 8201, scale 1:100 000. http://doi.org/10.4095/299711

Metsaranta, R.T. and Houlé, M.G., 2017d. Precambrian geology of the Highbank Lake area, "Ring of Fire" region, Ontario—Southern sheet; Ontario Geological Survey, Preliminary Map P.3806 (also Geological Survey of Canada, Open File 8202), scale 1:100 000. http://doi.org/10.4095/299712.

Metsaranta, R.T. and Houlé, M.G. 2020. Precambrian Geology of the McFaulds Lake "Ring of Fire" Region, Northern Ontario; Ontario Geological Survey, Open File Report 6359, 260 p.

Nixon, G.T., Manor, M.J., Jackson-Brown, S., Scoates, J.S., and Ames, D.E., 2015. Magmatic Ni-Cu-PGE sulphide deposits at convergent margins; *in* Targeted Geoscience Initiative 4: Canadian Nickel-Copper-Platinum Group Elements-Chromium Ore Systems — Fertility, Pathfinders, New and Revised Models, (ed.) D.E. Ames and M.G. Houlé; Geological Survey of Canada, Open File 7856, p. 17–34.

Nixon, G.T., Scoates, J.S., Milidragovic, D., Nott, J., Moerhuis, N., Ver Hoeve, T.J., Manor, M.J., and Kjarsgaard, I.M., 2020. Convergent margin Ni-Cu-PGE-Cr ore systems: U-Pb petrochronology and environments of Cu-PGE versus Cr-PGE mineralization in Alaskan-type intrusions; *in* Targeted Geoscience Initiative 5: Advances in the understanding of Canadian Ni-Cu-PGE and Cr ore systems – Examples from the Midcontinent Rift, the Circum-Superior Belt, the Archean Superior Province, and Cordilleran Alaskan-type intrusions, (ed.) W. Bleeker and M.G. Houlé; Geological Survey of Canada, Open File 8722, p. 197–218. https://doi.org/10.4095/326897

Pagé, P., Barnes, S.-J., Méric, J., and Houlé, M.G., 2015. Geochemical composition of chromite from Alexo komatiite in the western Abitibi greenstone belt: Implications for mineral exploration; *in* Targeted Geoscience Initiative 4: Canadian Nickel-Copper-Platinum Group Elements-Chromium Ore Systems — Fertility, Pathfinders, New and Revised Models, (ed.) D.E. Ames and M.G. Houlé; Geological Survey of Canada, Open File 7856, p. 187–195.

Pilkington, M. and Keating, P., 2015. Gravity gradiometer data analysis in mineral exploration; *in* Targeted Geoscience Initiative 4: Canadian Nickel-Copper-Platinum Group Elements-Chromium Ore Systems — Fertility, Pathfinders, New and Revised Models, (ed.) D.E. Ames and M.G. Houlé; Geological Survey of Canada, Open File 7856, p. 167–173.

Sappin, A.-A. and Houlé, M.G., 2020. The composition of magnetite in Archean mafic-ultramafic intrusions within the Superior Province; *in* Targeted Geoscience Initiative 5: Advances in the understanding of Canadian Ni-Cu-PGE and Cr ore systems – Examples from the Midcontinent Rift, the Circum-Superior Belt, the Archean Superior Province, and Cordilleran Alaskan-type intrusions, (ed.) W. Bleeker and M.G. Houlé; Geological Survey of Canada, Open File 8722, p. 181–196. https://doi.org/10.4095/326896

Sappin, A.-A., Houlé, M.G., Lesher, C.M., Metsaranta, R.T., and McNicoll, V.J., 2015a. Regional characterization of mafic-ultramafic intrusions in the Oxford-Stull and

Uchi domains, Superior Province, Ontario; *in* Targeted Geoscience Initiative 4: Canadian Nickel-Copper-Platinum Group Elements-Chromium Ore Systems — Fertility, Pathfinders, New and Revised Models, (ed.) D.E. Ames and M.G. Houlé; Geological Survey of Canada, Open File 7856, p. 75–85.

Sappin, A.-A., Houlé, M.G., Goutier, J., and McNicoll, V., 2015b. Caractérisation pétrographique et géochimique de la Pyroxénite de Baie Chapus, Baie-James: Un exemple de minéralisation en Fe-Ti-V dans la Province du Supérieur; Geological Survey of Canada, Open File 7745, 1 sheet, https://doi.org/10.4095/295612

Sappin, A.-A., Houlé, M.G. and Clark, T., 2018. Minéralisations en Ni-Cu-(EGP) dans la Province de Grenville: État des connaissances et nouvelles perspectives; Commission géologique du Canada, Présentation scientifique 78, 1 fichier.pdf. https://doi.org/10.4095/306387

Shahabi Far, M., Samson, I.M., Gagnon, J.E., Linnen, R.L., Good, D.J., and Ames, D.E., 2015. Textural character and chemistry of plagioclase and apatite in the Marathon Cu-PGE deposit, Ontario: Implications for mineralizing processes; *in* Targeted Geoscience Initiative 4: Canadian Nickel-Copper-Platinum Group Elements-Chromium Ore Systems — Fertility, Pathfinders, New and Revised Models, (ed.) D.E. Ames and M.G. Houlé; Geological Survey of Canada, Open File 7856, p. 233–243.

Smith, J., Bleeker, W., Liikane, D.A., Hamilton, M., Cundari, R., and Hollings, P., 2019. Characteristics of Ni-Cu-PGE sulphide mineralization within the 1.1 Ga Midcontinent Rift; *in* Targeted Geoscience Initiative: 2018 report of activities, (ed.) N. Rogers; Geological Survey of Canada, Open File 8549, p. 421–432. https://doi.org/10.4095/313676

Smith, J.W., Bleeker, W., Hamilton, M., Petts, D., Kamo, S.L., and Rossell, D., 2020. Timing and controls on Ni-Cu-PGE mineralization within the Crystal Lake Intrusion, 1.1 Ga Midcontinent Rift; *in* Targeted Geoscience Initiative 5: Advances in the understanding of Canadian Ni-Cu-PGE and Cr ore systems – Examples from the Midcontinent Rift, the Circum-Superior Belt, the Archean Superior Province, and Cordilleran Alaskan-type intrusions, (ed.) W. Bleeker and M.G. Houlé; Geological Survey of Canada, Open File 8722, p. 37–63. https://doi.org/10.4095/326881

Spath, C.S. III, Lesher, C.M., and Houlé, M.G., 2015. Hybridized ultramafic rocks in the Black Label hybrid zone of the Black Thor intrusive complex, McFaulds Lake greenstone belt, Ontario; *in* Targeted Geoscience Initiative 4: Canadian Nickel-Copper-Platinum Group Elements-Chromium Ore Systems — Fertility, Pathfinders, New and Revised Models, (ed.) D.E. Ames and M.G. Houlé; Geological Survey of Canada, Open File 7856, p. 103–114.

Trevisan, B.E., Hollings, P., Ames, D.E., and Rayner, N.M., 2015. The petrology, mineralization, and regional context of the Thunder mafic to ultramafic intrusion, Midcontinent Rift, Thunder Bay, Ontario; *in* Targeted Geoscience Initiative 4: Canadian Nickel-Copper Platinum Group Elements-Chromium Ore Systems — Fertility, Pathfinders, New and Revised Models, (ed.) D.E. Ames and M.G. Houlé; Geological Survey of Canada, Open File 7856, p. 139–149.

Zuccarelli, N., Lesher, C.M., and Houlé, M.G., 2018a. Sulphide textural variations and multiphase ore emplacement in the Eagle's Nest Ni-Cu-(PGE) deposit, McFaulds Lake greenstone belt, Ontario; *in* Targeted Geoscience Initiative: 2017 report of activities, volume 2, (ed.) N. Rogers; Geological Survey of Canada, Open File 8373, p. 29–34. https://doi.org/10.4095/306598

Zuccarelli, N., Lesher, C.M., Houlé, M.G., and Weston, R., 2018b. Textural variations in the Eagle's Nest Ni-Cu-(PGE) deposit in Ontario and implications for magma dynamics in a blade-shaped dike; Geological Survey of Canada, Scientific Presentation 83, 1 sheet, https://doi.org/10.4095/308255

Zuccarelli, N., Lesher, C.M., Houlé, M.G., and Barnes, S.J., 2020. Variations in the textural facies of sulphide minerals in the Eagle's Nest Ni-Cu-(PGE) deposit, McFaulds Lake greenstone belt, Superior Province, Ontario: Insights from microbeam scanning energy-dispersive X-ray fluorescence spectrometry; *in* Targeted Geoscience Initiative 5: Advances in the understanding of Canadian Ni-Cu-PGE and Cr ore systems – Examples from the Midcontinent Rift, the Circum-Superior Belt, the Archean Superior Province, and Cordilleran Alaskan-type intrusions, (ed.) W. Bleeker and M.G. Houlé; Geological Survey of Canada, Open File 8722, p. 165–179. https://doi.org/10.4095/326895

THESES

Brzozowski, M.J., 2018. Applications of mineral chemistry to petrogenesis and exploration in conduit-type Cu-PGE deposits; Ph.D. thesis, University of Windsor, Windsor, Ontario, 301 p.

Carson, H.J.E., in prep. Stratigraphy, geochemistry, and petrogenesis of the Black Thor intrusion and associated Cr and Ni-Cu-PGE mineralization, McFaulds greenstone belt, Ontario; Ph.D. thesis, Laurentian University, Sudbury, Ontario.

Davey, S.C., 2019. Testing the paleogeography of late Archean supercraton Superia using pre-breakup 2.51–1.98 Ga dyke and sill provinces—with a focus on the relationship between the Karelia-Kola and Superior cratonic fragments; Ph.D. thesis, Carleton University, Ottawa, Ontario, 313 p.

Farhangi, N., in prep. Mineralogy, geochemistry, and petrogenesis of Ni-Cu-(PGE) mineralization in the Black Thor intrusion, McFaulds Lake greenstone belt, Ontario; M.Sc. thesis, Laurentian University, Sudbury, Ontario.

Hiebert, R.S., 2018. Contamination of mafic to ultramafic magmas by sulfur-bearing sediments: evaluation of the environment of deposition and tracing the unique signature of the contaminants through the magma using multiple sulfur and iron isotope data; Ph.D. thesis, University of Manitoba, Winnipeg, Manitoba, 167 p.

Laudadio, A., 2019. 3-D Geological Modelling of the Double Eagle – Black Thor Intrusive Complexes, McFaulds Lake Greenstone Belt, Ontario, Canada; M.Sc. thesis, Carleton University, Ottawa, Ontario, 107 p.

MacInnis, L., 2019. Constraining alteration in the footwall of the Sudbury igneous complex: a case study of the alteration footprint to the Podolsky, Cu(-Ni)-PGE deposit, Sudbury; M.Sc. thesis, Laurentian University, Sudbury, Ontario, 204 p.

McKevitt, D.J., in prep. Localization of Ni-Cu-(PGE) mineralization in an early Proterozoic trans-crustal dike-sill-lava channel system, Cape Smith Belt, Nunavik; Ph.D. thesis, Laurentian University, Sudbury, Ontario.

Mehrmanesh, K., in prep. Stratigraphy of the Black Label Chromitite Horizon, Black Thor intrusion, McFaulds Lake Greenstone Belt, Ontario, Canada; M.Sc. thesis, Laurentian University, Sudbury, Ontario.

Méric, J., 2018. Le ruthénium (Ru), iridium (Ir), osmium (Os) et rhodium (Rh) et les éléments traces dans des chromites de komatiites issues de la zone Alexo et de la zone Hart, (Abitibi, Ontario): un outil diagnostique pour l'exploration de systèmes fertiles; M.Sc. thesis, Université du Québec à Chicoutimi, Saguenay, Québec, 185 p.

Paré, A., 2019. Origine d'un gabbro minéralisé issu de carottes de forages provenant de la Zone 5-8 de la Mine Raglan, Nunavik, Québec; B.Sc., Université Laval, Québec, Québec, 33 p.

Shahabi Far, M., 2016. The magmatic and volatile evolution of gabbros hosting the Marathon PGE-Cu deposit: Evolution of a conduit system; Ph.D. thesis, University of Windsor, Windsor, Ontario, 240 p.

Spath, C.S., III, 2017. Geology and Genesis of Hybridized Ultramafic Rocks in the Black Label Hybrid Zone of the Black Thor Intrusive Complex, McFaulds Lake Greenstone Belt, Ontario, Canada; M.Sc. thesis, Laurentian University, Sudbury, Ontario, 94 p.

Zuccarelli, N., in prep. Sulfide textural variations and multiphase ore emplacement in the Eagle's Nest Ni-Cu-(PGE) deposit, McFaulds Lake greenstone belt, Superior Province, Ontario, Canada; M.Sc. thesis, Laurentian University, Sudbury, Ontario.